Journal Pre-proof

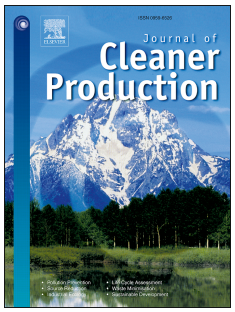

A Mathematical Model for Optimum Design and Synthesis of a Hybrid Electrolyser-Fuel Cell System: Production of Hydrogen and Freshwater from Seawater

Melisha Singh, Peter Mukoma, Brian North, Thokozani Majozi

PII: S0959-6526(20)33944-5

DOI: https://doi.org/10.1016/j.jclepro.2020.123899

Reference: JCLP 123899

To appear in: *Journal of Cleaner Production*

Received Date: 8 March 2020

Revised Date: 12 August 2020

Accepted Date: 20 August 2020

Please cite this article as: Singh M, Mukoma P, North B, Majozi T, A Mathematical Model for Optimum Design and Synthesis of a Hybrid Electrolyser-Fuel Cell System: Production of Hydrogen and Freshwater from Seawater, *Journal of Cleaner Production*, https://doi.org/10.1016/j.jclepro.2020.123899.

CRediT author statement

Melisha Singh: Conceptualization, Methodology, Data curation, Software, Writing- Original draft preparation, Visualization, Investigation, Validation, Writing- Reviewing and Editing.

Brian North: Conceptualization, Methodology, Supervision, Software, Investigation, Data curation, Validation, Visualization, Writing- Reviewing and Editing.

Peter Mukoma: Conceptualization, Methodology, Supervision, Software, Investigation, Data curation, Validation, Visualization, Writing- Reviewing and Editing.

Thokozani Majozi: Conceptualization, Methodology, Supervision, Software, Investigation, Data curation, Validation, Visualization, Writing- Reviewing and Editing.

HIGHLIGHTS

- This research aims to tackle the water and energy crisis affecting many countries.
- Uses H_2 evolved from seawater electrolysis to generate power and water in fuel cell.
- Provides an optimisation model of a hybrid seawater electrolyser-fuel cell system.
- An overall power conversion efficiency of 41.2 % and H_2O recovery rate of 48.2 %.
- Provides insight into an alternate clean energy conversion and H_2O purification system.

A Mathematical Model for Optimum Design and Synthesis of a Hybrid Electrolyser-Fuel Cell System: Production of Hydrogen and Freshwater from Seawater

Melisha Singh[a], Peter Mukoma[b], Brian North[b] and Thokozani Majozi[a,*]

[a] School of Chemical and Metallurgical Engineering, University of the Witwatersrand, 1 Jan Smuts Avenue, Braamfontein, Johannesburg, 2000, South Africa

[b] Council for Scientific and Industrial Research (CSIR), Meiring Naude Road, Brummeria, 0184, Pretoria, South Africa

[*]Corresponding author: thokozani.majozi@wits.ac.za; Tel: +27 11 717 7384;

Abstract

Fossil fuels have earned a reputation as unsustainable sources of energy, due to the release of carbon emissions that are attributable to global warming. To overcome the extensive release of carbon emissions into the environment, different approaches are being explored to produce energy, by replacing non-renewable fuels with renewable energy. Additionally, many countries across the world are emerging as water-scarce countries, due to the vulnerability of freshwater supply. This work, therefore, focuses on the design and synthesis of a hybrid electrolyser-fuel cell system to generate hydrogen and freshwater from seawater. The proposed system is designed to be integrated with a background process that requires both power and water. It has the potential to reduce the burden on freshwater sources and carbon footprint of background processes, as well as produce power. A one-dimensional, mathematical model is developed for a continuous hybrid seawater electrolyser-fuel cell system operated at steady state. The model determines the optimal operating conditions in terms of temperature, current density, electrode thickness and humidity, as well as the performance of the system through the activation overpotential, diffusion overpotential, ohmic overpotential and the open-circuit voltage. GAMS/BARON is used to optimise the hybrid system. Furthermore, a techno-economic evaluation is conducted to determine the viability of the system. Results indicate that an overall power conversion efficiency of 41.2 %, and a freshwater recovery rate of 48.2 % is achieved.

Keywords: Fuel cell; Electrolyser; Design; Synthesis; Hydrogen; Optimisation

A Mathematical Model for Optimum Design and Synthesis of a Hybrid Electrolyser-Fuel Cell System: Production of Hydrogen and Freshwater from Seawater

Melisha Singh[a], Peter Mukoma[b], Brian North[b] and Thokozani Majozi[a,*]

[a] School of Chemical and Metallurgical Engineering, University of the Witwatersrand, 1 Jan Smuts Avenue, Braamfontein, Johannesburg, 2000, South Africa

[b] Council for Scientific and Industrial Research (CSIR), Meiring Naude Road, Brummeria, 0184, Pretoria, South Africa

[*]Corresponding author: thokozani.majozi@wits.ac.za; Tel: +27 11 717 7384;

Abstract

Fossil fuels have earned a reputation as unsustainable sources of energy, due to the release of carbon emissions that are attributable to global warming. To overcome the extensive release of carbon emissions into the environment, different approaches are being explored to produce energy, by replacing non-renewable fuels with renewable energy. Additionally, many countries across the world are emerging as water-scarce countries, due to the vulnerability of freshwater supply. This work, therefore, focuses on the design and synthesis of a hybrid electrolyser-fuel cell system to generate hydrogen and freshwater from seawater. The proposed system is designed to be integrated with a background process that requires both power and water. It has the potential to reduce the burden on freshwater sources and carbon footprint of background processes, as well as produce power. A one-dimensional, mathematical model is developed for a continuous hybrid seawater electrolyser-fuel cell system operated at steady state. The model determines the optimal operating conditions in terms of temperature, current density, electrode thickness and humidity, as well as the performance of the system through the activation overpotential, diffusion overpotential, ohmic overpotential and the open-circuit voltage. GAMS/BARON is used to optimise the hybrid system. Furthermore, a techno-economic evaluation is conducted to determine the viability of the system. Results indicate that an overall power conversion efficiency of 41.2 %, and a freshwater recovery rate of 48.2 % is achieved.

Keywords: Fuel cell; Electrolyser; Design; Synthesis; Hydrogen; Optimisation

1. Introduction

The global supply of fossil fuels is rapidly declining due to the increase in energy demand. Naturally, the environment cannot replace fossil fuels at the rate at which they are being consumed by the growing human population. Consequently, as the demand for power increases, the environment and power grid faces numerous challenges in trying to meet the demands of the global population, and economy. This is related to the energy trilemma which tackles the conflicting goals of providing energy security, energy affordability and an environmentally sustainable energy supply (Rinkinen et al., 2019). Globally, 74.7% of the electricity generated is derived from fossil fuels, which addresses the affordability and security goals of the energy trilemma (International Energy Agency, 2019). However, it is incapable of meeting the environmental sustainability goal, on the account of greenhouse gas emissions that have detrimental effects on the environment.

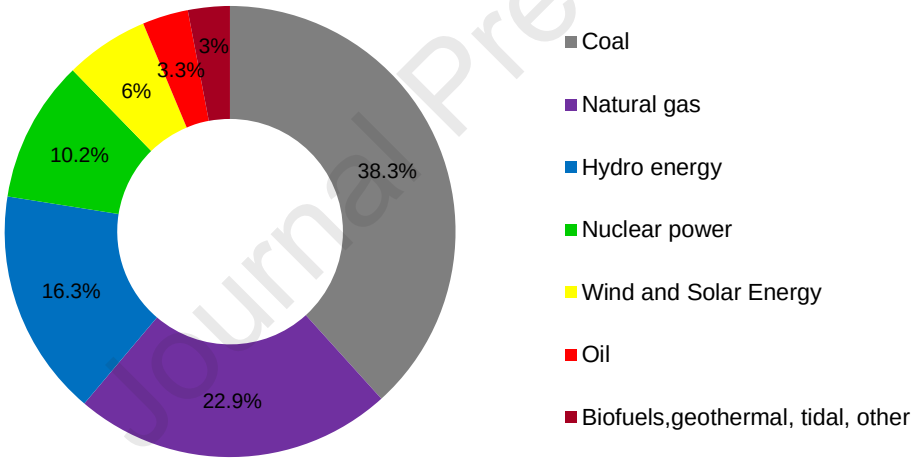

Figure 1: 2017 Global Electricity Production (International Energy Agency, 2019)

To address the energy crisis, it is imperative for power generation utilities to pursue alternate avenues for energy production leading to one of the biggest technological shifts experienced to date (Darras et al., 2015). This is attained by adopting the use of an energy system that harnesses energy from renewable energy sources, causes zero harm to the environment, is cost-effective, and is capable of ensuring the political and the economic security of the nation (Kimura et al., 2019).

As such, hydrogen (H_2) produced from renewable energy is gaining a substantial amount of attention as a promising substitute fuel, and an effective long-term energy storage medium. It has been identified to play an important role in sustainable energy production and will contribute to the transition towards a zero-carbon emission world. The versatility of hydrogen in applications, future low-cost potential, and its negligible harm to the environment classify H_2 as a clean fuel (Pierucci et al., 2017). Consequently, hydrogen together with fuel cell technology shows promise of addressing the energy trilemma.

According to published data, approximately 96% of the total hydrogen consumed in the world is currently produced from fossil fuels (AlZahrani and Dincer, 2017). Among these fossil fuels are coal and natural gas, which are used as primary feedstock to produce H_2 through gasification and reforming processes (López Ortiz et al., 2016). However, conventional fossil-fuel derived processes are associated with various environmental concerns that include, finite supply, excessive release of carbon emissions directly related to climate change, and global warming (Acar and Dincer, 2020). Consequently, the environmental concerns arising from using these processes have necessitated a shift towards producing hydrogen renewably, through electrolysers powered by hydro, solar, tidal and wind energy.

1.1. Electrolysis

Electrolysis is one of the most recognised methods of producing chemical products from their natural state. This is particularly true for the production of H_2 and oxygen (O_2) from freshwater and seawater. As seen in Figure 2, many countries across the world are experiencing water (H_2O) shortages, due to the continuously declining average rainfall. It is, therefore, an obvious advantage to pursue saline sources of H_2O when considering the production of renewable hydrogen. In view of the fact that seawater is an inexhaustible source of H_2O, as opposed to freshwater which has become constrained.

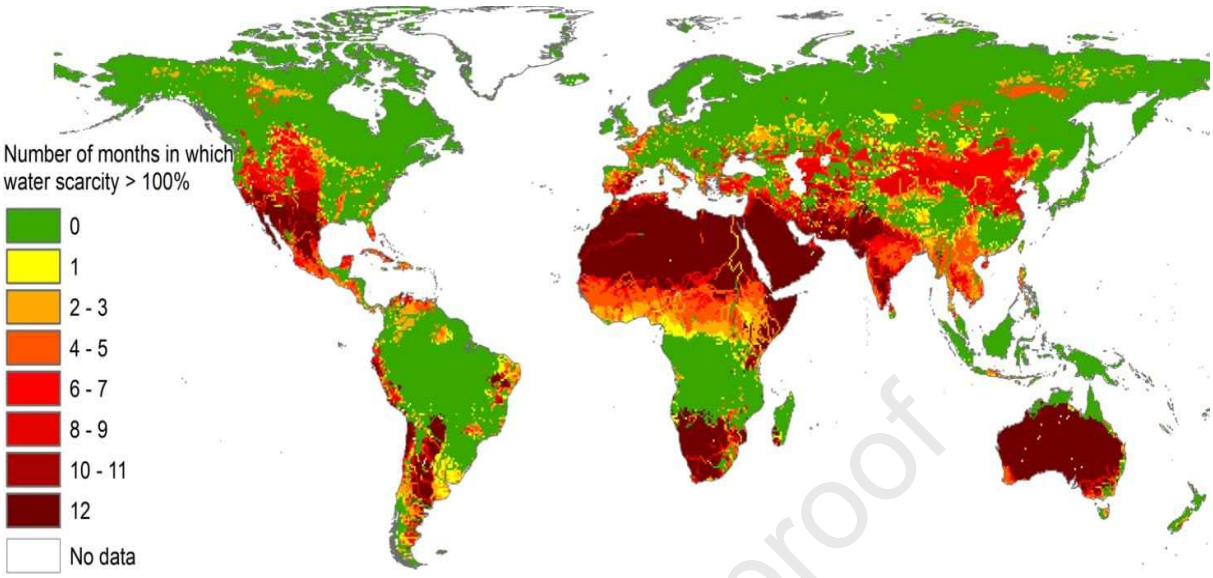

Figure 2: World Water Scarcity Map (Carylsue, 2016)

Over recent years, several experimental studies have been conducted for seawater electrolysis to determine the viability, efficiency, use of effective electrodes and catalysts to promote H_2 and O_2 evolution. More specifically, Abdel-Aal et al. (2010) presented an experimental study to determine the rate of H_2 and chlorine evolution from seawater electrolysis. Mohammad and Kaukhab (2011) investigated the use of sulphur electrodes to promote O_2 evolution and prevent the formation of magnesium hydroxide precipitation in an experimental study. Ravichandran et al. (2011) focused their research on investigating a selectively permeable electrode constructed from a sulfonated-polystyrene-ethylene-butylene-styrene membrane on an IrO_2 electrode, that was cationically selective towards O_2 evolution and repelled chlorine ions.

More recently, Srisiriwat and Pirom (2017) conducted an experimental study to determine the feasibility of a photovoltaic (PV)/seawater electrolyser/fuel cell system. In addition, Srisiriwat and Pirom (2017) proposed to simulate the system they had developed in 2017, in the Hybrid Optimisation Model for Electric Renewable (HOMER) simulation software to obtain the optimal design of the system as future work.

Lei et al. (2018) prepared a Nano-tungsten carbide composite electro-catalyst (AuPdPt-WC/C) to replace platinum catalysts in the hydrogen evolution reaction. In another experimental study, Kuang et al. (2019) developed a hierarchical anode with corrosion-resistance and O_2 evolution properties. The anode was fabricated from a nickel-iron hydroxide electrocatalyst coated uniformly on nickel sulfide layer which had been developed on porous nickel foam. In a similar study, Yu et al. (2019) presented an experimental study on a 3-D core-shell metal nitride catalyst which is constructed from NiFeN nanoparticle on NiMoN nanorods supported on nickel foam. The proposed NiMoN@NiFeN electrocatalyst was investigated to promote the O_2 evolution reaction and was used in an alkaline seawater electrolyser. In another study, Yan et al. (2019) conducted an investigation on improving the O_2 evolution efficiency and stability of various transition metals such as manganese, manganese+molybdenum, manganese+molybdenum+vanadium and manganese+iron+vanadium oxide coated electrodes, that were prepared a titanium substrate, and contained an iridium dioxide (IrO_2) intermediate layer.

In contrast to all the experimental work, Yang et al. (2019) presented a performance model for seawater electrolysis in an undivided cell (no membrane between anolyte and catholyte). Semi-empirical models were obtained for current density, cell voltage, total residual oxidant and energy consumption.

Although some work has been conducted in modelling the performance of a seawater electrolyser, the above-mentioned model is limited to seawater electrolysis in an undivided cell. Additionally, this model did not take into account diffusion overpotential, and optimisation of the seawater electrolyser was not performed.

1.2. Modelling PEM Electrolysers and Fuel Cells

Proton exchange membrane electrolysers (PEMEs) and proton exchange membrane fuel cells (PEMFCs) have been extensively modelled separately as clean energy conversion systems. In recent years, mathematical modelling of PEMEs has increased significantly and has been based upon PEMFC models.

An extensive literature review was conducted by Falcão and Pinto. (2020) on the various types of models that have been developed to predict the performance of a PEME. Analytical, empirical and semi-empirical models have been formulated. Han et al. (2015) developed a comprehensive one-dimensional freshwater electrolyser model, to determine the effect of varying operating conditions and design parameters on the performance of the cell. In that formulation, open-circuit voltage, activation overpotential, diffusion overpotential and ohmic overpotential are considered. Ni et al. (2006) proposed an electrochemical model to analyse the relationship between current density and voltage in a PEME. That model investigated the open-circuit voltage, activation overpotential, and the ohmic overpotential, but did not evaluate the effect of the diffusion overpotential. This was due to the insignificant effect of the mass transport limitations present in thin electrodes. In another study, Chanderis et al. (2015) developed a one-dimensional numerical model to analyse the effect of temperature and current density on the degradation of the PEM. They concluded that the cathode exhibited greater membrane degradation than the anode, and temperature had a significant impact on the cell performance. It is worth noting, all these models were limited to freshwater electrolysis.

Notable work for one-dimensional, isothermal fuel cells was done by Bernadi and Verbrugge (1991). That work was shortly extended by Springer et al. (1991). Later, researchers developed new models and made modifications to existing models to investigate the effects of membrane dehydration (Yang et al., 2019), membrane flooding (Mammar et al., 2019), and H_2O transport through the membrane (Lee et al., 2019).

According to the work conducted by Shekhar (2013), which compared one-dimensional and three-dimensional fuel cell models, one-dimensional models were found to be more cost-effective and useful for practical applications than three-dimensional models. Abdin et al. (2016) developed a one-dimensional mathematical model of a PEMFC in MATLAB-Simulink to explore the effect that humidification, pressure, partial pressure and temperature on the performance of the cell. They concluded that the relative humidity of the reactant gases influenced membrane hydration and resistance. Li and Lv (2018) presented a model on the combined effects of water transport on the performance of PEMFCs. In that work, a one-dimensional, two-phase flow, steady-state model was developed.

1.3. Models of Hybrid Systems

Hybrid energy systems have recently gained more attention as an effective renewable energy storage medium. Typically, these hybrid systems couple several renewable energy sources such as solar and wind energy (Lin et al., 2015). Numerous studies have been conducted on the design, modelling and optimisation of photovoltaic/fuel cell/wind turbine hybrid systems. Lin et al. (2015) developed a generic mathematical model to analyse the temporary operational flexibility of a solar/wind/PEMFC/battery hybrid system. Prieto-Prado et al. (2018) proposed an integrated system of wind, photovoltaic energy, electrolysers, fuel cells, hydrogen storage tanks, and a reverse osmosis plant to provide H_2O to the Canary Islands. That study used HOMER simulation software to determine the economic and technical feasibility of the power system.

Additionally, Tobaru et al. (2017) presented a novel 100% renewable energy system comprised of a PV array, wind generator, fuel cell, seawater electrolysis plant, and battery energy storage system (BESS) in a remote island in Japan. That system was compared to one that did not contain a seawater electrolysis plant and BESS. Additionally, mixed-integer linear programming was used to minimise the difference between the cost of equipment, and the revenue generated by the chemicals produced from seawater electrolysis.

Espinosa-Lȯpez et al. (2018) developed a semi-empirical, steady-state electrochemical model coupled with a dynamic lumped capacitance dynamic thermal model of a 46 kW high-pressure PEME. MATLAB-Simulink was used to develop the model and Particle-Swarm Optimisation was used to identify the parameters in the model.

In another study, Maleki (2018) presented a mathematical model for the design and optimisation of various hybrid renewable energy systems that included, a solar-wind-reverse osmosis desalination system, coupled with either a battery or hydrogen energy storage. A metaheuristic optimisation technique known as the bee's algorithm was proposed for the optimal design of the hybrid renewable energy systems. Liu et al. (2019) developed a model of a novel integrated energy system which contains multiple decentralised energy generation integrated systems with a centralised energy generation system to provide a stable supply of electricity. The capacity of the proposed hybrid energy system was optimised through the use of a superstructure-based mixed-integer non-linear programming (MINLP) model. GAMS was used to model the optimisation problem and BARON was used as the solver.

1.4. Research Motivation

According to the literature reviewed, many studies have been conducted on the development of individual mathematical models for freshwater PEME and PEMFCs. Additionally, numerous studies have been done on hybrid systems which couple various renewable energy sources, and have been optimised in HOMER. Research on seawater electrolysis has been extensively carried out but has merely been focused on experimental work, such as investigating the performance of different electrocatalysts and electrodes for the evolution of O_2, as well as efficiency and viability. However, to date, a comprehensive mathematical model for the optimal design of a one-dimensional seawater electrolyser has not yet been developed. Moreover, research on the development of a mathematical formulation for the optimum design of a hybrid electrolyser-fuel cell (HEFC) system, to produce H_2 and freshwater from seawater is limited. This work aims to determine the optimal design parameters and operating conditions, as well as the economic viability of the HEFC system. The industrial applicability will provide insight into the feasibility of integrating a HEFC system into a background process, especially in energy and water constrained regions.

Consequently, the aim of this paper is to tackle the water and energy crisis arising in many countries across the world, such as South Africa, which is the 30th driest country in the world (Gerbi, 2017), and where more than 90% of the electricity generated is sourced from coal (Ratshomo and Nembahe, 2016). This is achieved by eliminating the strain on freshwater bodies, producing renewable energy, and eliminating environmental concerns by providing a green energy conversion and water purification system. Integration of HEFC with the background process allows for generated power and freshwater to be fed directly or indirectly to the process, thereby reducing freshwater and power requirements. This research will focus on developing a mathematical model for the design and synthesis of a HEFC system to produce hydrogen and freshwater from seawater. A nonlinear programming (NLP) formulation is presented. It determines the maximum power conversion efficiency achievable in the hybrid system. The model developed provides a framework to analyse the performance of the hybrid system, and a method of exploring variables that are difficult to measure in a physical system. Furthermore, an economic evaluation is carried out to determine the viability of the proposed system.

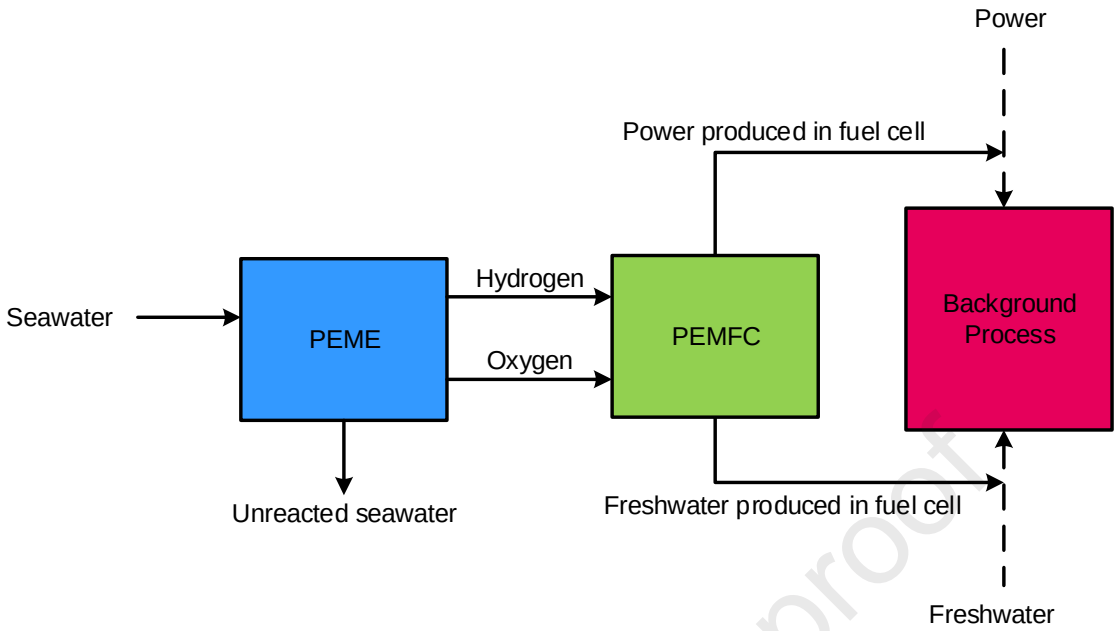

Figure 3: HEFC System Integrated with a Background Process

This paper is organised into 6 sections. The first section gives the introduction to the paper. The second section describes the problem being addressed. The third section presents the methodology development of the proposed HEFC system, which includes the detailed mathematical model. The fourth section demonstrates the application of the HEFC mathematical model in an illustrative example. This is followed by the results and discussion in the fifth section. Lastly, the sixth section summarises the research conclusions.

2. Problem Statement

The 21st century is one of the most challenging times for humankind, as greenhouse gases pose huge concerns on the environment, as well as human health. Moreover, many countries across the world are emerging as water-scarce countries, as well as experiencing an energy-crisis due to the increase in energy demand. To alleviate pollution from fossil fuel-based energy production, the H_2 economy is explored. H_2 is a promising alternative energy carrier and a viable solution to decentralise the production of energy from oil and fossil fuels. Therefore, to tackle the energy and water crisis, a HEFC system is presented to produce H_2 and freshwater from seawater. A mathematical model will be developed for the optimum design and synthesis of the HEFC system and will be formulated as an NLP optimisation problem. The advantages associated with the HEFC system include the following:

i) Reduced strain of freshwater bodies and fresh feed water required by the background process
ii) Supplementary power available for use within the background process
iii) System is 100% environmentally friendly (no carbon emissions released)
iv) In countries where water and power are constrained, the HEFC system will effectively utilise available seawater to provide power and freshwater to processes
v) Low pressure operation (atmospheric) compared to membrane technology used in desalination
vi) Reduced capital cost and limited seawater pretreatement required
vii) Onsite desalination and power production allows the chemical plant to operate off the grid

The problem being addressed in this paper may be formally stated as follows:

Given:

i) A set of units, *P*, composed of an electrolyser stack and fuel cell stack
ii) A set of electrolyser cells, *M*, with a known number of cells in the electrolyser stack
iii) A set of fuel cells, *N*, with a known number of cells in the fuel cell stack
iv) A fixed flowrate of seawater entering the electrolyser stack, N_{H_2O}
v) Source of energy used in the electrolyser
vi) Type of electrolyser and fuel cell being used

The objective is to determine the optimal performance and design conditions that maximise the power conversion efficiency.

3. Methodology Development

The mathematical model developed in this paper integrates the design and synthesis of a PEME system and a PEMFC system. A comprehensive mathematical formulation that aims to simultaneously produce hydrogen and freshwater from seawater is presented and is used to determine the optimal performance, design conditions and economic viability of the system. The aforementioned concept is achieved through the use of seawater electrolysers and hydrogen fuel cells.

3.1. Systematic Approach

To develop the optimisation model for the HEFC system, the approach illustrated in Figure 4 is followed. Firstly, a superstructure of the system is developed. The NLP model is based on the superstructure and is used to explore all the possible combinations for the optimisation problem. The overall superstructure for the HEFC system is given in Figure 5. As illustrated in Figure 5, electrolysers and fuel cells are used to produce H_2 and freshwater from seawater. The energy required to power the electrolyser may be supplied by solar, wind, tidal or hydro energy. This power is supplied to a set of *M* electrolysers, where it is consumed and used to split seawater molecules into H_2 and O_2. All the H_2 and O_2 formed in the electrolyser stack are then sent to a set of *N* fuel cells where the H_2 and O_2 react to form freshwater. Electrons flow through an external circuit from the anode to the cathode. This transfer of electrons generates power. Unreacted H_2 and O_2 in one fuel cell flow into the next cell in the stack, where they are reacted until all the reactants are consumed

After the development of the superstructure, the hybrid system is divided into two sub-models, viz. the seawater electrolyser and the H_2 fuel cell. In developing a mathematical model for the seawater electrolyser and the hydrogen fuel cell, each sub-model is broken down into three components, viz. voltage, membrane and material balance components. All potential losses present in the electrolyser and fuel cell sub-models are modelled in the voltage component. H_2O concentration and transport are modelled in the membrane component for each of the sub-models. The mass and molar balance for H_2, O_2 and H_2O in the electrolyser and the fuel cell are modelled in the material balance component. Thereafter, performance equations for each seawater electrolyser and hydrogen fuel cell sub-model are given in the formulation of system constraints.

It should be noted that the seawater electrolyser is initially modelled as a freshwater electrolyser. Modifications are made by altering the parameters to suit the electrolysis of seawater. The seawater electrolyser model with the objective function of minimising power consumed is solved to determine the feasibility of the model. In contrast, H_2 fuel cell sub-model with the objective function of maximising power produced is solved to determine the feasibility of the model. Lastly, once each sub-model has been modelled, solved and deemed feasible, mass balance constraints are included to integrate the seawater electrolyser sub-model and fuel cell sub-model. This integrated model is then solved and the optimal design parameters are obtained and used to size the internal components of the HEFC system. This is followed by the techno-economic evaluation of the HEFC system based on the optimal variables obtained from the optimised integrated HEFC system model. For the techno-economic evaluation, the annual cash flow, net present value, payback period and internal rate of return are calculated to determine the viability of the proposed system.

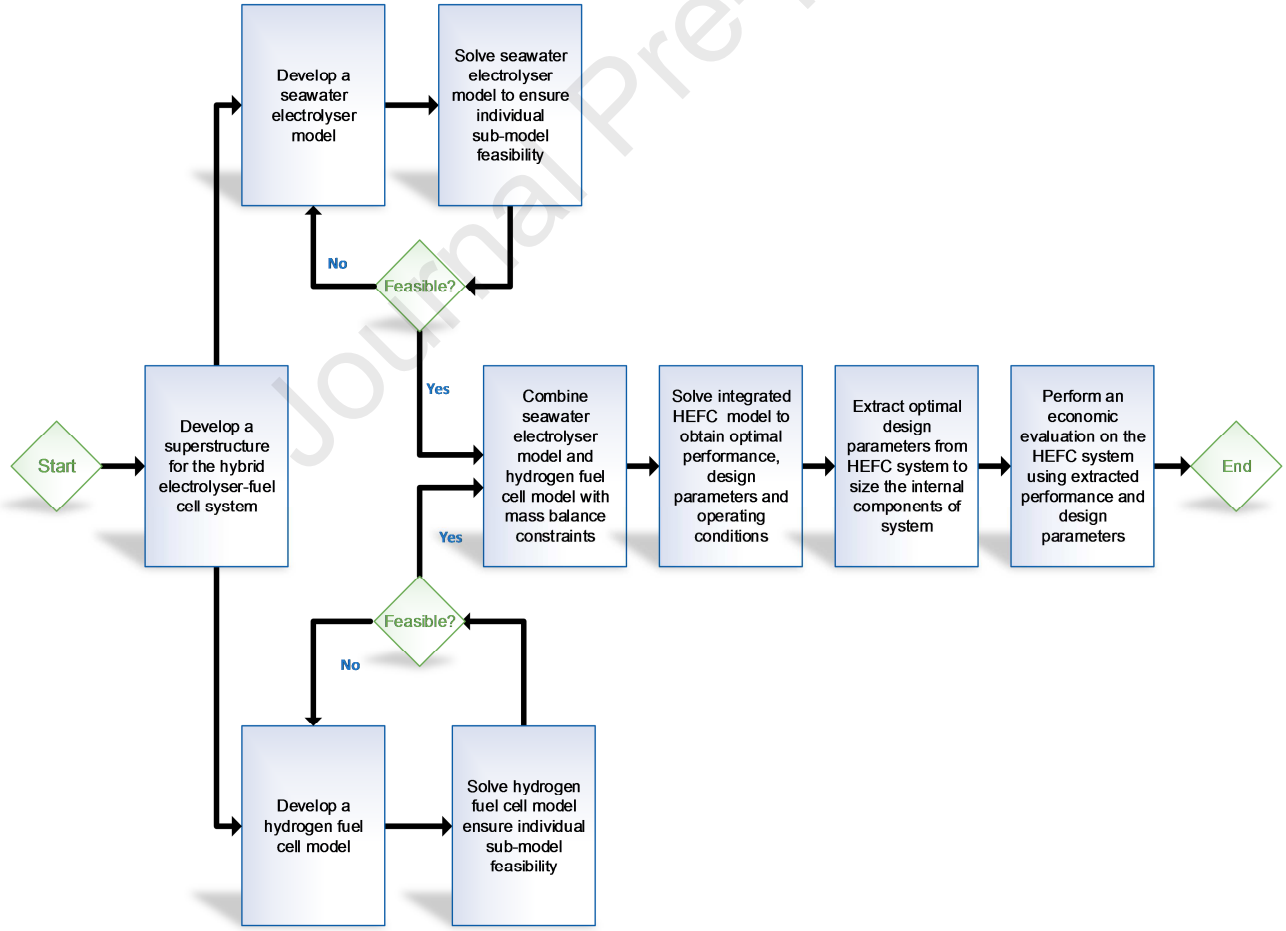

Figure 4: HEFC System Schematic Approach

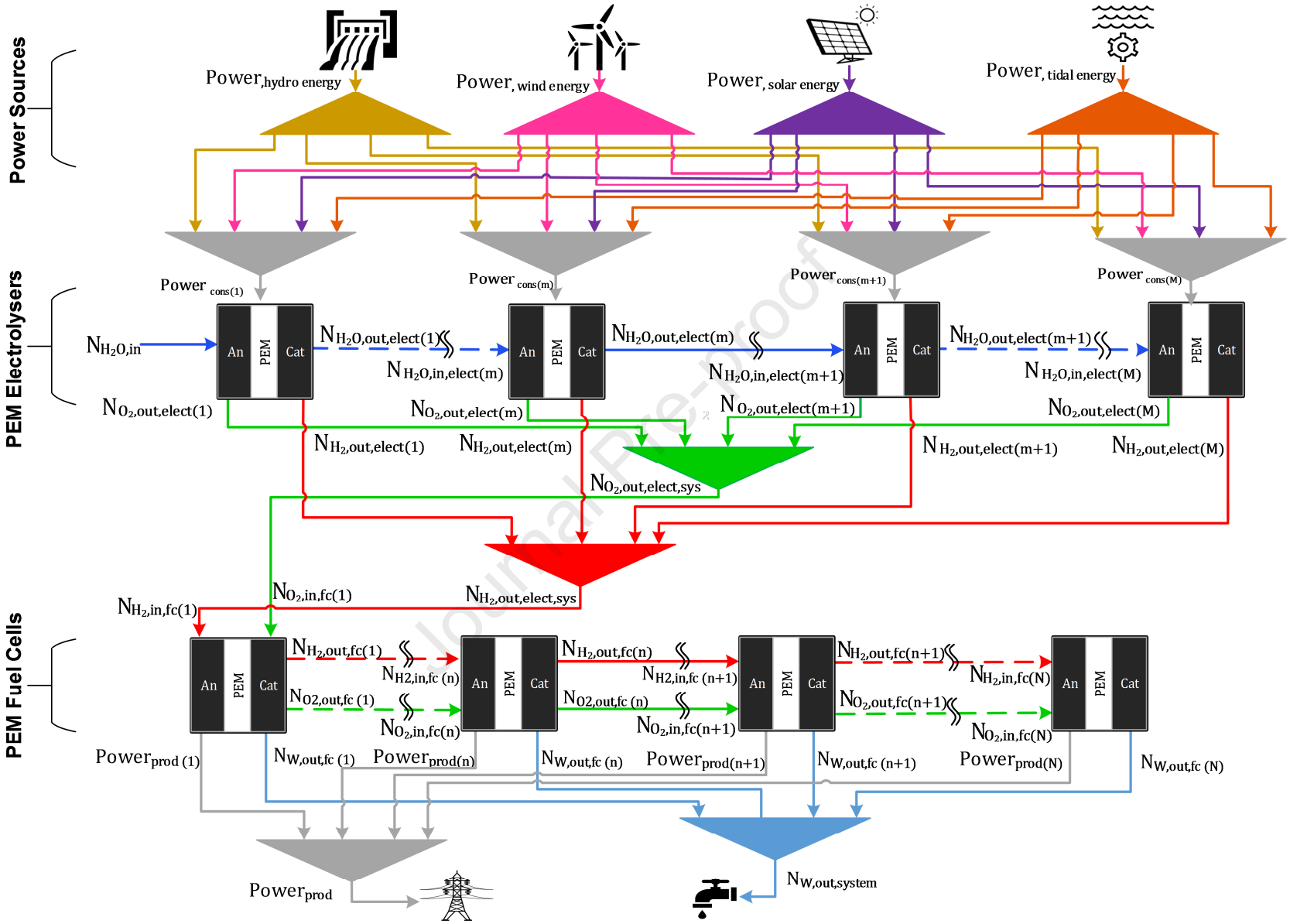

Figure 5: HEFC System Superstructure

3.2. Electrolyser and Fuel Cell Operation

In the electrolyser, seawater is fed to the anode where it is oxidised to form O_2. H^+ ions flow from the anode through a Nafion electrolyte membrane to a platinum cathode where H_2 gas is formed. In seawater electrolysis, chlorine evolves at the anode instead of O_2. However, in this model, the evolution of O_2 is promoted through the use of a nano-tungsten carbide electro-catalyst and a magnesium hydroxide anode. Chlorine leaves the electrolyser as a solution with the brine and excess seawater. Reaction (1)-(2) describe the reactions that take place in the seawater electrolyser. A schematic diagram of a PEME is shown in Figure 6 (Han et al., 2015).

Anode: $$H_2O \rightarrow \frac{1}{2}O_2 + 2e^- + 2H^+ \quad (1)$$

Cathode: $$2H^+ + 2e^- \rightarrow H_2 \quad (2)$$

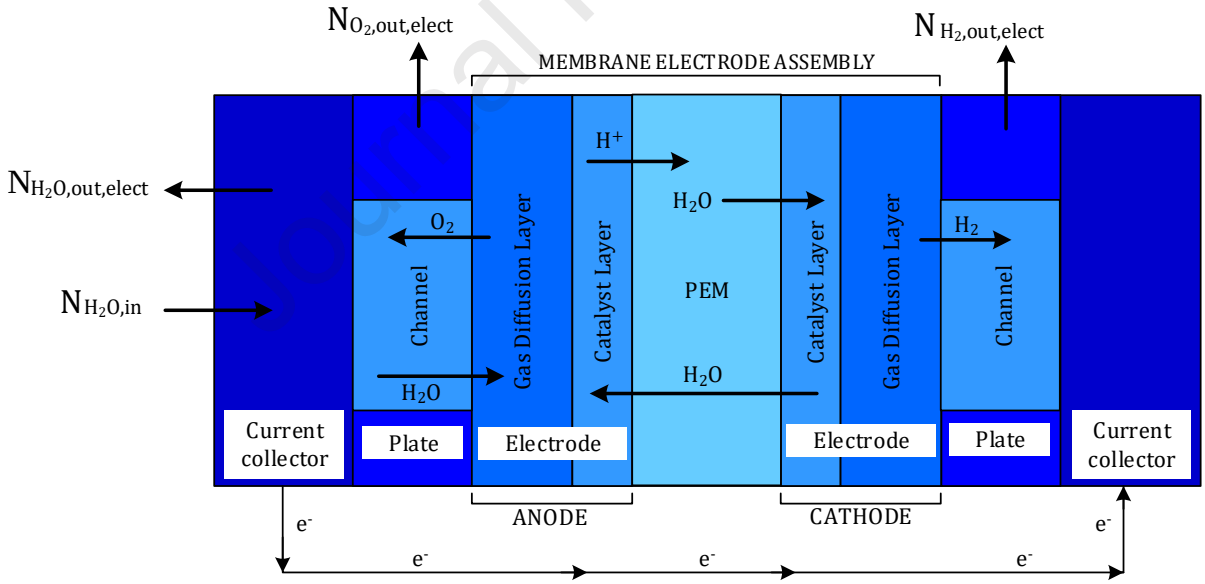

Figure 6: Schematic Diagram of a PEME

In the fuel cell, H_2 fed to the anode is oxidised and the O_2 fed to the cathode is reduced to form freshwater. Figure 7 illustrates a schematic diagram of a PEMFC (Abdin et al., 2015).

$$\text{Anode:} \qquad H_2 \rightarrow 2H^+ + 2e^- \tag{3}$$

$$\text{Cathode:} \qquad \frac{1}{2}O_2 + 2e^- + 2H^+ \rightarrow H_2O \tag{4}$$

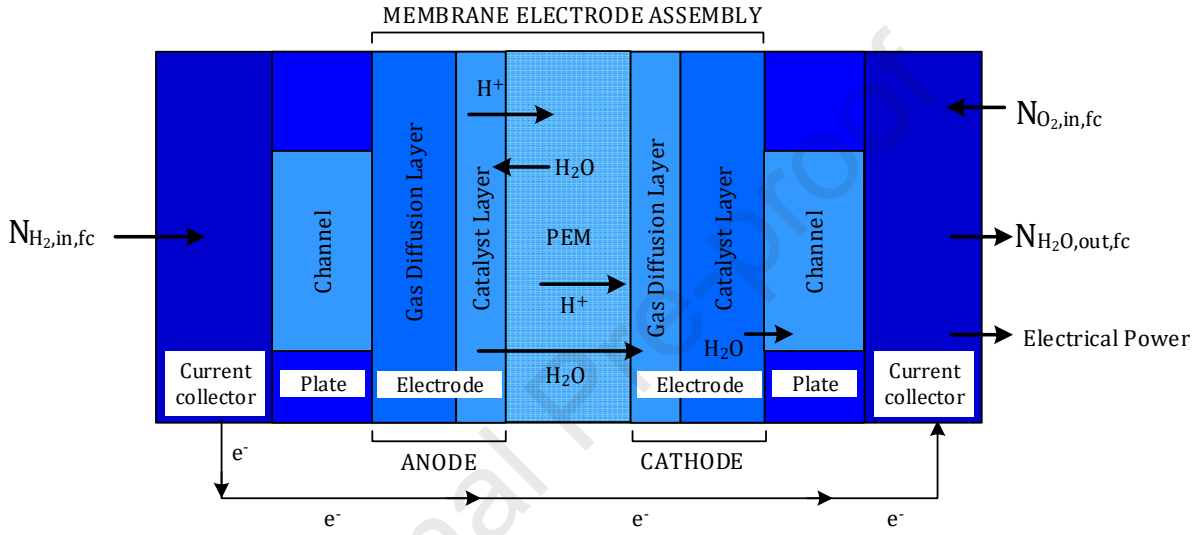

Figure 7: Schematic Diagram of a PEMFC

3.3. Voltage Component

The seawater electrolyser model is adapted from the models developed by Marangio et al. (2009) and Han et al. (2015). Modifications are made to these models by altering the current density, charge transfer coefficient, exchange current density and the input voltage required to suit seawater electrolysis. Additionally, the H_2 fuel cell modelled in this system is adapted from the model proposed by Abdin et al. (2016). Most mathematical expressions presented in the electrolyser models are identical to the expressions in the fuel cell, with the exception that H_2 is present in the anode and O_2 in the cathode of the fuel cell, as opposed to the electrolyser where H_2 is present in the cathode and O_2 in the anode. Adjustments are then made to take this into account.

The performance of the electrolyser and the fuel cell is measured via the current and voltage of each unit. Since the cells are connected in series, the current in each cell of the electrolyser stack remains the same. This assumption also holds for the fuel cell stack. Subsequently, this section describes the performance of the HEFC system.

3.3.1. Current

Current in the electrolyser and fuel cell stack is dependent on the reaction area and the current density. Where I is current, A is the reaction area and j is the current density.

$$I(p) = A(p) * j(p) \qquad \forall\, p \in P \tag{5}$$

3.3.2. Open Circuit Voltage

The open-circuit voltage (OCV) is theoretically known as the minimum voltage when all other overpotentials are not taken into consideration. The reversible voltage describes the voltage obtained if the system experiences no voltage losses, and all Gibbs free energy could be converted to electrical energy (Han et al., 2015). Equation (6) describes the OCV derived from the Nernst equation at standard pressure. T is the operating temperature in Kelvin, R is the gas constant, z is the number of electrons transferred during the reaction, F is Faraday's constant (96 485 mol/C) and β_i is the partial pressure of species i.

$$V_{OCV}(p) = 1.229 - 0.9 * 10^{-3}(T(p) - 298) + \frac{RT(p)}{zF}\ln\left(\frac{\beta_{H_2}\beta_{O_2}^{0.5}}{\beta_{H_2O}}\right) \qquad \forall\, p \in P \tag{6}$$

3.3.3. Activation Overpotential

Activation overpotential is derived from the Butler-Volmer equation and is defined as the potential loss due to the electrochemical reaction. It is the voltage used to drive the chemical reaction at the anode and cathode, and determines the rate at which the electrochemical reactions take place at the surface of the electrode. It is influenced by chemical and physical parameters, viz. temperature, pressure, active reaction site, catalyst property and electrode morphology.

$$V_{act}(p) = \frac{RT(p)}{\alpha_{an}F} * ln\left[\left(\frac{j\,(p)}{2j_{o,an(p)}}\right) + \sqrt{\left(\frac{j(p)}{2j_{o,an(p)}}\right)^2 + 1}\,)\right] + \frac{RT(p)}{\alpha_{cat}F} * ln\left[\left(\frac{j(p)}{2j_{o,cat(p)}}\right) + \sqrt{\left(\frac{j(p)}{2j_{o,cat(p)}}\right)^2 + 1}\,)\right] \quad \forall\, p \in P, p = electrolyser \tag{7}$$

$$V_{act}(p) = \frac{RT(p)}{\alpha_{an}F} * ln\left(\frac{j\,(p)}{j_{o,an(p)}}\right) + \frac{RT(p)}{\alpha_{cat}F} * ln\left(\frac{j(p)}{j_{o,cat(p)}}\right) \quad \forall\, p \in P, p = fuel\ cell \tag{8}$$

$$V_{act}(p) = V_{act,an}(p) + V_{act,cat}(p) \qquad \forall\, p \in P \tag{9}$$

Where α_{an} and α_{cat} are the anode and cathode charge transfer coefficients. $j_{o,an}$ and $j_{o,cat}$ are the exchange current density of the anode and cathode. $V_{act,an}$, $V_{act,cat}$ and V_{act} are the anode, cathode and overall activation overpotentials.

3.3.4. Diffusion Overpotential

The diffusion overpotential is also known as the concentration overpotential, and is defined as the potential loss due to the mass transport limitations within the membrane-electrode interface. The mass transport of H_2, O_2 and H_2O through the porous electrode is governed by Fick's law. Typically, diffusion overpotential plays a major role in electrolysers when the surface of the membrane becomes heavily populated with O_2 gas bubbles, and the rate of the reaction is reduced. Similarly, in fuel cells, O_2 bubbles present prevent the flow of H^+ ions to the cathode. This hinders the H_2O formation reaction and consequently reduces the performance of the fuel cell (Abdin et al., 2016).

Equations (10) to (12) describe the anode, cathode and total diffusion overpotential in the electrolyser. In fuel cells, the anode of the electrolyser becomes the cathode and vice versa.

$$V_{diff,an}(p) = \frac{R\,T(p)}{4F} ln \frac{C_{O_2,me}(p)}{C_{O_2,me,o}(p)} \qquad \forall\, p \in P, p = electrolyser \tag{10}$$

$$V_{diff,cat}(p) = \frac{R\,T(p)}{2F} ln \frac{C_{H_2,me}(p)}{C_{H_2,me,o}(p)} \qquad \forall\, p \in P, p = electrolyser \tag{11}$$

$$V_{diff}(p) = V_{diff,an}(p) + V_{diff,an}(p) \qquad \forall\, p \in P \tag{12}$$

Where $C_{O_2,me}$ and $C_{H_2,me}$ are the concentration of O_2 and H_2 at the electrode-membrane interface. $C_{O_2,me,o}$ and $C_{H_2,me,o}$ are the concentration of oxygen and H_2 at the electrode-membrane interface at reference conditions. $V_{diff,an}$, $V_{diff,cat}$ and V_{diff} are the anode, cathode and overall diffusion overpotentials.

3.3.5. Ohmic Overpotential

The ohmic overpotential is the resistance due to the transfer of electrons through the membrane, electrode, plates and interconnectors present in the electrolyser and the fuel cell. Typically, ohmic overpotential is comprised of two resistances, viz. electrical and ionic. The electrical resistance is due to the flow of electrons through an electrically conductive component.

In contrast, the ionic resistance is caused by the flow of H^+ ions in the membrane. Bernardi and Verbrugge (1991) found that ionic resistances contributed significantly to the ohmic overpotential.

Due to a large number of unknowns in the electrodes and bipolar plates, the ohmic overpotential in this paper only takes into account ionic resistances. The protonic conductivity of the membrane is calculated as a function of H_2O content. It is expressed in the empirical equation proposed by Springer et al. (1993). σ_{mem} is the membrane conductivity, V_{ohm} is the ohmic overpotential, δ_{mem} is the thickness of the membrane and λ_{mem} is the membrane humidity degree.

$$\sigma_{mem}(p) = (0.5139\lambda_{mem}(p) - 0.326)\exp\left(1\,268\left(\frac{1}{303} - \frac{1}{T(p)}\right)\right) \qquad \forall\, p \in P \qquad (13)$$

$$V_{ohm}(p) = \delta_{mem}(p)\left[\frac{I(p)}{A(p)\,\sigma_m(p)}\right] \qquad \forall\, p \in P \qquad (14)$$

3.3.6. Total Voltage

The input voltage of the electrolyser cell is expressed in Equation (15) as the sum of the open-circuit voltage, activation, diffusion and ohmic overpotentials. In contract, the output voltage of the fuel cell stack is expressed in Equation (16) as the difference between the open-circuit voltage, activation, diffusion and ohmic overpotentials.

$$V(p) = V_{OCV}(p) + V_{act}(p) + V_{diff}(p) + V_{Ohm}(p)$$
$$\forall\, p \in P,\ p = electrolyser \qquad (15)$$

$$V(p) = V_{OCV}(p) - V_{act}(p) - V_{diff}(p) - V_{Ohm}(p)$$
$$\forall\, p \in P, p = fuel\ cell \qquad (16)$$

3.3.7. Seawater Density and Viscosity

The density and viscosity of seawater are taken as a function of temperature and salinity. An equation of state and experimental data adapted from the study conducted by El-Dessouky and Ettouney (2002), is used to determine the density and viscosity of seawater in the temperature range of 10-180℃, and salinity from 0-160 ppt (parts per thousand). Equation (17) expresses the density of seawater, where ρ_w is the density of H_2O, and D_i and F_i are constants. Equation (18) gives the viscosity of seawater, where μ_{H_2O} is the viscosity of H_2O, μ_r is the relative viscosity of H_2O and μ_{sw} is the viscosity of seawater

$$\rho_w = (D_1F_1 + D_2F_2 + D_3F_3 + D_4F_4) * 10^3 \qquad (17)$$

$$\mu_{sw} = \left(\mu_{H_2O}\right)(\mu_R) * 10^{-3} \qquad (18)$$

3.3.8. Concentration in the Anode-Membrane and Cathode-Membrane Interface

To determine the concentration gradient present on either side of the membrane, the concentration is taken as a function of H_2O content. The H_2O activity, anode and cathode humidity degree, and the electrode concentration expressions are derived from the model presented by Shimpalee and Van Zee (2007). Equations (19) and (20) describe the activity of H_2O in the anode-membrane interface and cathode-membrane interface. Where $A_{H_2O.an}$ and $A_{H_2O,cat}$ are the H_2O activities in the anode and cathode. y_{H_2O} is the H_2O molar composition, P is the operating pressure and P_{sat} is the saturated vapour pressure.

$$A_{H_2O.an}(p) = \frac{y_{H_2O,an}(p) * P(p)}{P_{sat}(p)} \qquad \forall\, p \in P \tag{19}$$

$$A_{H_2O.cat}(p) = \frac{y_{H_2O,cat}(p) * P(p)}{P_{sat}(p)} \qquad \forall\, p \in P \tag{20}$$

Equation (21) expresses the saturated vapour pressure of H_2O, which is a function of temperature (Log, 2018).

$$P_{sat}(\mathrm{p}) = 611e^{\frac{19.65(\mathrm{T(p)}-273.15)}{\mathrm{T(p)}}} \qquad \forall\, p \in P \tag{21}$$

The molar compositions of H_2O at the anode and cathode of the electrolyser are given in Equations (22) and (23). Where $n_{H_2O,an}$ is the molar flux of H_2O at the anode, $n_{H_2O,cat}$ is the molar flux of H_2O at the cathode, n_{O_2} is the molar flux of O_2 and n_{H_2} is the molar flux of H_2.

$$y_{H_2O,an}(p) = \frac{n_{H_2O,an}(p)}{n_{H_2O,an}(p) + n_{O_2}(p)} \qquad \forall\, p \in P,\ p = electrolyser \tag{22}$$

$$y_{H_2O,cat}(p) = \frac{n_{H_2O,cat}(p)}{n_{H_2O,cat}(p) + n_{H_2}(p)} \qquad \forall\, p \in P, p = electrolyser \tag{23}$$

Equations (24) and (25) express the molar composition of H_2O at the anode and cathode of the fuel cell.

$$y_{H_2O,an}(p) = \frac{n_{H_2O,an}(p)}{n_{H_2O,an}(p)+n_{H_2}(p)} \qquad \forall\, p \in P,\ p = fuel\ cell \qquad (24)$$

$$y_{H_2O,cat}(p) = \frac{n_{H_2O,cat}(p)}{n_{H_2O,cat}(p)+n_{O_2}(p)} \qquad \forall\, p \in P,\ p = fuel\ cell \qquad (25)$$

The molar flux of H_2O at the anode and cathode of the electrolyser is given in Equations (26) and (27), whereas the molar flux of H_2O in the fuel cell are given in Equations (28) and (29).

$$n_{H_2O,an}(p) = \frac{\dot{N}_{H_2O,cons}+\dot{N}_{H_2O.mem}(p)}{A(p))} \qquad \forall\, p \in P,\ p = electrolyser \qquad (26)$$

$$n_{H_2O,cat(p)} = \frac{\dot{N}_{H_2O.mem}(p)}{A(p)} \qquad \forall\, p \in P,\ p = electrolyser \qquad (27)$$

$$n_{H_2O,an}(p) = \frac{\dot{N}_{H_2O.mem}(p)}{A(p))} \qquad \forall\, p \in P, p = fuel\ cell \qquad (28)$$

$$n_{H_2O,cat(p)} = \frac{\dot{N}_{H_2O,prod}-\dot{N}_{H_2O.mem}(p)}{A(p)} \qquad \forall\, p \in P, p = fuel\ cell \qquad (29)$$

Equations (30) and (31) express the molar flux of H_2 and O_2 in the electrolyser.

$$n_{H_2}(p) = \frac{\dot{N}_{H_2,prod}}{A(p)} \qquad \forall\, p \in P, p = electrolyser \qquad (30)$$

$$n_{O_2(p)} = \frac{\dot{N}_{O_2,prod}}{A(p)} \qquad \forall\, p \in P, p = electrolyser \qquad (31)$$

The H_2 and O_2 molar flux of the fuel cell is described in Equations (32) and (33).

$$n_{H_2}(p) = \frac{\dot{N}_{H_2,cons}}{A(p)} \qquad \forall\, p \in P,\ p = fuel\ cell \qquad (32)$$

$$n_{O_2(p)} = \frac{\dot{N}_{O_2,cons}}{A(p)} \qquad \forall\, p \in P,\ p = fuel\ cell \qquad (33)$$

The humidity of H_2O at the anode and the cathode under different H_2O activity conditions are given in Equations (34) to (37).

$$\lambda_{an}(p) = 14 + 1.4\,(A_{H_2O,an}(p) - 1) \quad 1 \le A_{H_2O,an} \le 3 \qquad \forall\, p \in P \qquad (34)$$

$$\lambda_{cat}(p) = 14 + 1.4\,(A_{H_2O,cat}(p) - 1) \quad 1 \le A_{H_2O,cat} \le 3 \qquad \forall\, p \in P \qquad (35)$$

$$\lambda_{an}(p) = 0.043 + 17.8 * A_{H_2O,an}(p) - 39.65 * A_{H_2O,an}(p)^2 + 36 * A_{H_2O,an}(p)^3$$
$$0 \le A_{H_2O,an} \le 1 \qquad \forall\, p \in P \qquad (36)$$

$$\lambda_{cat}(p) = 0.043 + 17.8 * A_{H_2O,cat}(p) - 39.65 * A_{H_2O,cat}(p)^2 + 36 * A_{H_2O,cat}(p)^3$$
$$0 \le A_{H_2O,cat} \le 1 \qquad \forall\, p \in P \qquad (37)$$

Where λ_{an} and λ_{cat} are the anode and cathode humidity degrees. Equation (38) describes the membrane humidity degree as the average anode and cathode humidity degree.

$$\lambda_{mem}(p) = \frac{\lambda_{an}(p) + \lambda_{cat}(p)}{2} \qquad \forall\, p \in P \qquad (38)$$

Equations (39) to (40) describe the concentration of H_2O at the membrane-electrode interface of the anode and the cathode in the electrolyser. $\rho_{mem,dry}$ is the dry density of the membrane and $M_{mem,dry}$ is the molecular mass of the dry membrane.

$$C_{H_2O,me,an}(p) = \frac{\rho_{m,dry}}{M_{m,mem,dry}} \lambda_{an}(p) \quad \forall\, p \in P,\ p = electrolyser \qquad (39)$$

$$C_{H_2O,me,cat}(p) = \frac{\rho_{m,dry}}{M_{m,mem,dry}} \lambda_{cat}(p) \quad \forall\, p \in P, p = electrolyser \qquad (40)$$

The concentration of H_2O at the membrane-electrode interface of the anode and cathode of the fuel cell are given in Equations (41) and (42). δ_{an} and δ_{cat} are the anode and cathode thickness. $D_{eff,an}$ and $D_{eff,cat}$ are the anode and cathode effective diffusion coefficients. MW_{H_2O} is the molecular weight of water.

$$C_{H_2O,me,an}(p) = \left(\frac{\rho_{H_2O}{}^{*}T_{(p)}}{MW_{H_2O}}\right) - \left(\frac{\delta_{an}(p)*n_{H_2O,an}(p)}{D_{eff,an}}\right) \quad \forall\, p \in P, p = fuel\ cell \tag{41}$$

$$C_{H_2O,me,cat}(p) = \left(\frac{\rho_{H_2O}{}^{*}T_{(p)}}{MW_{H_2O}}\right) + \left(\frac{\delta_{cat}(p)*n_{H_2O,cat}(p)}{D_{eff,cat}}\right) \forall\, p \in P, p = fuel\ cell \tag{42}$$

Equations (43) and (44) give the H_2 and O_2 channel concentration of the electrolyser. $C_{H_2,ch}$ and $C_{O_2,ch}$ are the concentrations of H_2 and O_2 at the channel. $y_{H_2,ch}$ and $y_{O_2,ch}$ are the molar compositions of H_2 and O_2 at the channel.

$$C_{H_2,ch}(p) = \frac{P_{cat}(p)* y_{H_2,ch}(p)}{RT(p)} \qquad \forall\, p \in P, p = electrolyser \tag{43}$$

$$C_{O_2,ch}(p) = \frac{P_{an}(p)* y_{O_2,ch}(p)}{RT(p)} \qquad \forall\, p \in P, p = electrolyser \tag{44}$$

The concentration of H_2 and O_2 at the channel of the fuel cell is given in Equations (45) and (46).

$$C_{H_2,ch}(p) = \frac{P_{an}(p)* y_{H_2,ch}(p)}{RT(p)} \qquad \forall\, p \in P, p = fuel\ cell \tag{45}$$

$$C_{O_2,ch}(p) = \frac{P_{cat}(p)* y_{O_2,ch}(p)}{RT(p)} \qquad \forall\, p \in P, p = fuel\ cell \tag{46}$$

At reference conditions, the H_2 and O_2 molar concentrations at the membrane and channel of the electrolyser are given by Equations (47) to Equation (50). $C_{H_2,me,o}$ and $C_{O_2,me,o}$ are the concentrations of H_2 and O_2 at the membrane under reference conditions. $C_{H_2,ch,o}$ and $C_{O_2,ch,o}$ are the concentrations of H_2 and O_2 at the channel under reference conditions. T_{ref} and P_{ref} are the reference temperature and pressure.

$$C_{O_2,me,o}(p) = C_{O_2,ch,o}(p) + \frac{\delta_{an}(p) * n_{O_2}(p)}{D_{eff,an}(p)} \quad \forall\, p \in P, p = electrolyser \quad (47)$$

$$C_{H_2,me,o}(p) = C_{H_2,ch,o}(p) + \frac{\delta_{cat}(p) * n_{H_2}(p)}{D_{eff,cat}(p)} \quad \forall\, p \in P, p = electrolyser \quad (48)$$

$$C_{O_2,ch,o}(p) = \frac{P_{ref} y_{O_2(p)}}{RT_{ref}} \quad \forall\, p \in P, p = electrolyser \quad (49)$$

$$C_{H_2,ch,o}(p) = \frac{P_{ref} y_{H_2(p)}}{RT_{ref}} \quad \forall\, p \in P, p = electrolyser \quad (50)$$

In the fuel cell, the molar concentrations of H_2 and O_2 at the membrane and the channel are described in Equations (51) to (54).

$$C_{H_2,me,o}(p) = C_{H_2,ch,o}(p) + \frac{\delta_{an}(p) * n_{H_2}(p)}{D_{eff,an}(p)} \quad \forall\, p \in P, p = fuel\ cell \quad (51)$$

$$C_{O_2,me,o}(p) = C_{O_2,ch,o}(p) + \frac{\delta_{cat}(p) * n_{O_2}(p)}{D_{eff,cat}(p)} \quad \forall\, p \in P,\ p = fuel\ cell \quad (52)$$

$$C_{H_2,ch,o}(p) = \frac{P_{ref} y_{H_2(p)}}{RT_{ref}} \quad \forall\, p \in P, p = fuel\ cell \quad (53)$$

$$C_{O_2,ch,o}(p) = \frac{P_{ref} y_{O_2(p)}}{RT_{ref}} \quad \forall\, p \in P, p = fuel\ cell \quad (54)$$

Equations (55) to (58) describe the molar composition of H_2 and O_2 in the channel of the electrolyser and the fuel cell.

$$y_{H_2,ch}(p) = \frac{n_{H_2}(p)}{n_{H_2O,cat}(p)+n_{H_2}(p)} \qquad \forall\, p \in P, p = electrolyser \quad (55)$$

$$y_{O_2,ch}(p) = \frac{n_{O_2}(p)}{n_{H_2O,an}(p)+n_{O_2}(p)} \qquad \forall\, p \in P, p = electrolyser \quad (56)$$

$$y_{H_2,ch}(p) = \frac{n_{H_2}(p)}{n_{H_2O,an}(p)+n_{H_2}(p)} \qquad \forall\, p \in P, p = fuel\ cell \quad (57)$$

$$y_{O_2,ch}(p) = \frac{n_{O_2}(p)}{n_{H_2O,cat}(p)+n_{O_2}(p)} \qquad \forall\, p \in P, p = fuel\ cell \quad (58)$$

According to Equation (59) and Equation (60), the effective diffusion coefficients of the H_2-H_2O mixture and O_2-H_2O mixtures are functions of porosity, percolation and diffusion coefficient of the mixture. Equations (61) and (62) give the diffusion coefficients for the H_2-H_2O mixture and the O_2-H_2O mixture.

$$D_{eff,H_2-H_2O}(p) = D_{H_2-H_2O}(p)\varepsilon\left(\frac{\varepsilon-\varepsilon_p}{1-\varepsilon_p}\right)^{\tau} \qquad \forall\, p \in P \quad (59)$$

$$D_{eff,O_2-H_2O}(p) = D_{O_2-H_2O}(p)\varepsilon\left(\frac{\varepsilon-\varepsilon_p}{1-\varepsilon_p}\right)^{\tau} \qquad \forall\, p \in P \quad (60)$$

$$D_{H_2-H_2O}(p) = a\left(\frac{T(p)}{\sqrt{T_{cr,H_2}T_{cr,H_2O}}}\right)^{b}\left(P_{cr,H_2}P_{cr,H_2O}\right)^{\frac{1}{3}}\left(T_{cr,H_2}T_{cr,H_2O}\right)^{\frac{5}{12}}\left(\frac{1}{MW_{H_2}}+\frac{1}{MW_{H_2O}}\right)^{\frac{1}{2}} \qquad \forall\, p \in P \quad (61)$$

$$D_{O_2-H_2O}(p) = a\left(\frac{T}{\sqrt{T_{cr,O_2}T_{cr,H_2O}}}\right)^{b}\left(P_{cr,O_2}P_{cr,H_2O}\right)^{\frac{1}{3}}\left(T_{cr,O_2}T_{cr,H_2O}\right)^{\frac{5}{12}}\left(\frac{1}{MW_{O_2}}+\frac{1}{MW_{H_2O}}\right)^{\frac{1}{2}} \qquad \forall\, p \in P \quad (62)$$

Where $D_{H_2-H_2O}$ and $D_{O_2-H_2O}$ are the diffusion coefficients of the H_2-H_2O mixture and the O_2-H_2O mixture. ε is the electrode porosity, ε_p is the Percolation threshold (0.11), τ is the empirical coefficient (τ = 0.785), a and b are the empirical coefficients ($a = 3.64 \times 10^{-4}$ and $b = 2.334$), P_{cr} is the critical pressure, T_{cr} is the critical temperature and MW_{H_2} and MW_{O2} are the molecular weights of hydrogen and oxygen.

3.4. Membrane Component

Mass transport plays a fundamental role in the membrane and is responsible for the formation of H_2, O_2 and H_2O. The driving force in the membrane is due to the flow of H_2O. It occurs in three forms as described below and illustrated in Figure 8 (Han et al., 2015).

(i) Flow due to the electro-osmotic drag

(ii) Flow due to the pressure gradient across the PEM from the cathode to the anode

(iii) Flow due to the concentration difference

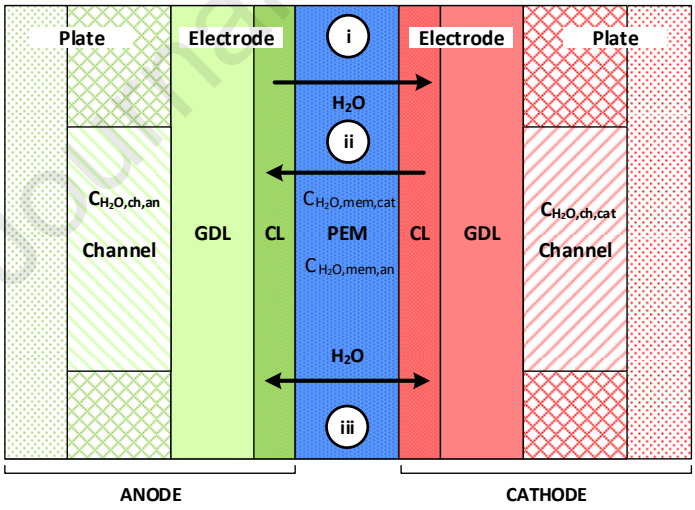

Figure 8: Water Transport through the PEM

The flow of H_2O due to the concentration gradient across the PEM is calculated in Equation (63). $\dot{N}_{H_2O,grad}$ is the molar flow rate of H_2O due to the concentration gradient and D_w is the diffusion coefficient of H_2O inside the membrane.

$$\dot{N}_{H_2O,grad}(p) = \frac{A(p)D_w}{\delta_{mem}(p)}\left[C_{H_2O,me,cat}(p) - C_{H_2O,me,an}(p)\right] \quad \forall\, p \in P \tag{63}$$

The electro-osmotic drag is the transportation of H_2O molecules from the anode to the cathode, as a result of the flux of hydrated protons flowing through the membrane. $\dot{N}_{H_2O,eo}$ is the molar flow rate due to the electro-osmotic drag and n_d is the electro-osmotic drag coefficient.

$$\dot{N}_{H_2O,eo}(p) = n_d(p) * \frac{I(p)}{F} \quad \forall\, p \in P \tag{64}$$

The H_2O flow rate due to the pressure difference across the membrane is expressed in Equation (65). $\dot{N}_{H_2O,pe}$ is the molar flow rate due to the pressure effect and K_{darcy} is the permeability coefficient of H_2O. ρ_{H_2O}, μ_{H_2O} and M_{m,H_2O} are the density, viscosity and molecular weight of H_2O.

$$\dot{N}_{H_2O,pe}(p) = K_{darcy}\frac{A(p)\rho_{H_2O}}{\mu_{H_2O}M_{m,H_2O}} \quad \forall\, p \in P \tag{65}$$

The net flow rate of H_2O through the membrane is expressed in Equation (66). It describes the flow rate of H_2O that is transported through the membrane ($\dot{N}_{H_2Omem}$), as the sum of H_2O due to the concentration gradient, electro-osmotic drag and the pressure effect.

$$\dot{N}_{H_2O,mem}(p) = \dot{N}_{H_2O,grad}(p) + \dot{N}_{H_2O,eo}(p) - \dot{N}_{H_2O,pe}(p) \quad \forall\, p \in P \tag{66}$$

3.5. Material Balance Constraints

3.5.1 Water Balance

As seen in Figure 9a, seawater enters at the electrolyser at the anode where it is consumed. In a similar manner, the fuel cell system (Figure 9b) works in a reverse way; H_2O is produced in the cathode. In both the electrolyser and fuel cell, H_2O flows through the PEM to keep membrane hydrated.

(9a)

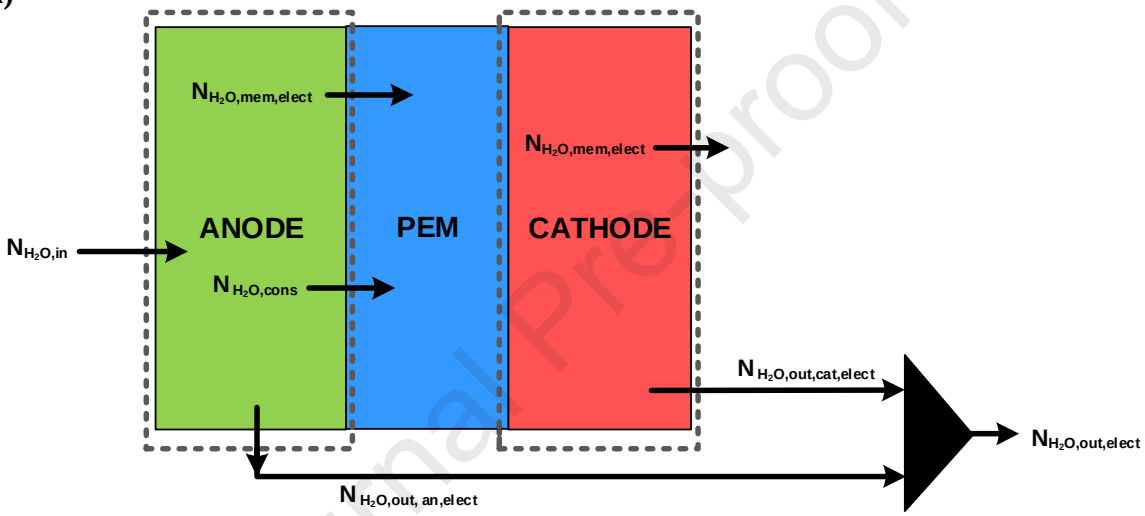

(9b)

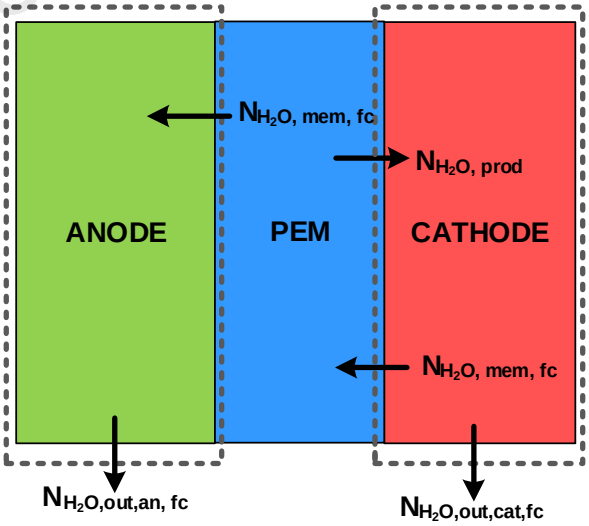

Figure 9: Water Balance across the Electrolyser (9a) and Fuel Cell (9b)

Equation (67) states that the molar flow rate of seawater entering the electrolyser is equal to the H_2O entering the anode of the first electrolyser cell. The molar flow rate of H_2O consumed $\dot{N}_{H_2O,cons}$ is given in Equation (68).

$$\dot{N}_{H_2O,in} = \dot{N}_{H_2O,in,an,elect}(m) \qquad \forall\, m \in M, m = 1 \tag{67}$$

$$\dot{N}_{H_2O,cons} = \frac{I(p)}{2F} \qquad \forall\, p \in P, p = electrolyser \tag{68}$$

Equation (69) states that the molar flow rate of H_2O leaving the electrolyser is equal to the difference between the molar flow rate of H_2O entering the anode, being consumed and the amount of H_2O flowing through the membrane.

$$\dot{N}_{H_2O,out,an,elect}(m) = \dot{N}_{H_2O,in,an,elect}(m) - \dot{N}_{H_2O,cons} - \dot{N}_{H_2O,mem,elect} \qquad \forall\ m \in M \tag{69}$$

Equation (70) gives the flowrate of H_2O leaving the cathode of the electrolyser cell.

$$\dot{N}_{H_2O,out,cat,elect}(m) = \dot{N}_{H_2O,mem,elect} \qquad \forall\, m \in M \tag{70}$$

The total flow rate of H_2O leaving a cell in the electrolyser is given in Equation (71)

$$\dot{N}_{H_2O,out,elect}(m) = \dot{N}_{H_2O,out,an,elect}(m) + \dot{N}_{H_2O,out,cat,elect}(m) \qquad \forall\ m \in M \tag{71}$$

Equation (72) describes the molar flow rate of H_2O entering the next anode cell as the molar flow rate of H_2O leaving the previous cell.

$$\dot{N}_{H_2O,in,an,elect}(m) = \dot{N}_{H_2O,out,elect}(m-1) \qquad \forall\ m \in M, m > 1 \tag{72}$$

Equation (73) describes the total molar flow rate leaving the electrolyser system.

$$\dot{N}_{H_2O,out,elect,sys} = \sum \dot{N}_{H_2O,out,elect}\,(m) \qquad \forall\, m \in M \tag{73}$$

The molar flow rate of H_2O produced in the fuel cell is given in Equation (74).

$$\dot{N}_{H_2O,prod} = \frac{I(p)}{2F} \qquad \forall\, p \in P, p = fuel\ cell \tag{74}$$

Equation (75) and Equation (76) express the molar flow rate of H_2O leaving the anode and cathode of the fuel cell.

$$\dot{N}_{H_2O,out,an,fc}(n) = \dot{N}_{H_2O,mem,fc} \qquad \forall\, n \in N \tag{75}$$

$$\dot{N}_{H_2O,out,cat,fc}(n) = \dot{N}_{H_2O,prod} - \dot{N}_{H_2O,mem,fc} \qquad \forall\, n \in N \tag{76}$$

Equation (77) gives the overall mass balance for the PEME system.

$$M_{H_2O,in} = M_{H_2O,out,elect,sys} + M_{H_2,out,elect,sys} + M_{O_2,Oout,elect,sys} \tag{77}$$

Equation (78) describes the mass balance for the PEMFC system and states that the mass of H_2O, H_2 and O_2 leaving the fuel cell must equal the mass of H_2 and O_2 entering the fuel cell.

$$M_{H_2O,out,fc,sys} + M_{H_2,out,fc,sys} + M_{O_2,out,fc,sys} = M_{H_2,in,fc}(n) + M_{O_2,in,fc}(n) \qquad \forall\, n \in N, n = 1 \tag{78}$$

Equation (79) states that the total mass of H_2O leaving the electrolyser and fuel cell systems must be equal to the mass of seawater entering.

$$M_{H_2O,in} = M_{H_2O,out,elect,sys} + M_{H_2O,out,fc,sys} \tag{79}$$

3.5.2. Oxygen Balance

The PEM only allows protons to flow through the membrane. Therefore all hydroxide and O^{2-} ions remain within the anode compartment of the electrolyser. O_2 is formed and leaves from the anode. No O_2 is found within the cathode. On the contrary, in fuel cells, O_2 enters the fuel cell at the cathode, where it reacts to form H_2O. Figure 10 graphically illustrates the O_2 balance in the electrolyser and fuel cell.

(10a)

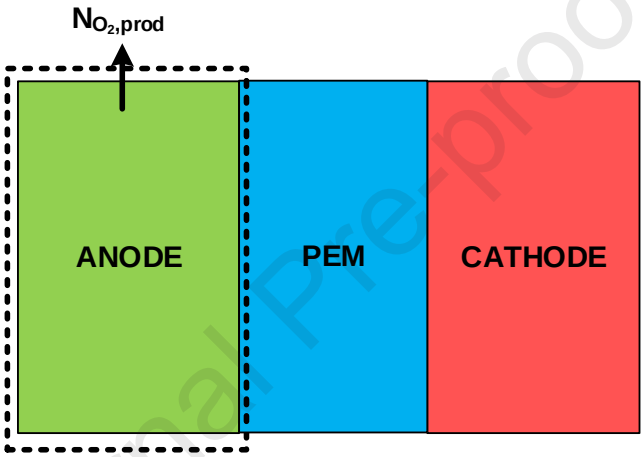

(10b)

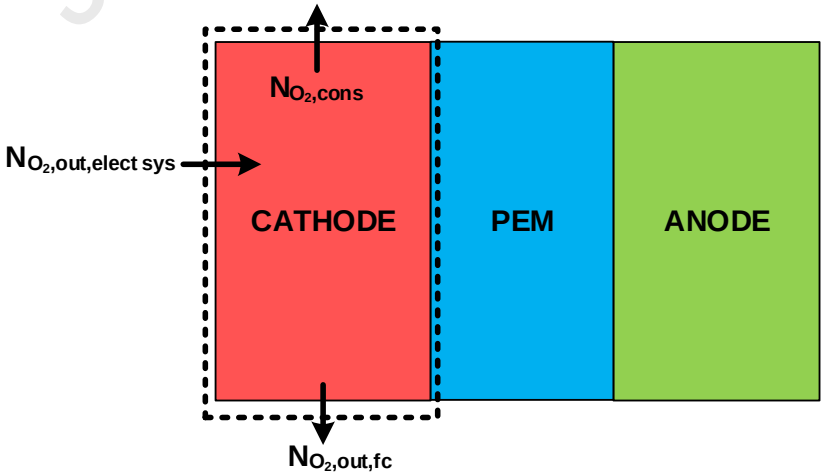

Figure 10: Oxygen Balance across the Electrolyser (10a) and Fuel Cell (10b)

Equation (80) expresses the molar flow rate of O_2 produced in the electrolyser. Equation (81) and (82) describe the molar flow rate of O_2 leaving the anode, and a cell in the electrolyser stack. Equation (83) gives the total O_2 leaving the electrolyser system.

$$\dot{N}_{O_2,prod} = \frac{I(p)}{4F} \qquad \forall\, p \in P, p = electrolyser \tag{80}$$

$$\dot{N}_{O_2,out,an,elect}(m) = \dot{N}_{O_2,prod} \qquad \forall\, m \in M \tag{81}$$

$$\dot{N}_{O_2,out,elect}\,(m) = \dot{N}_{O_2,out,an,elect}(m) \qquad \forall\ m \in M \tag{82}$$

$$\dot{N}_{O_2,out,elect,sys} = \sum \dot{N}_{O_2,out,elect}(m) \qquad \forall\ m \in M \tag{83}$$

Equation (84) states that the total molar flow rate of O_2 leaving the electrolyser system is equal to the molar flow rate of O_2 entering the first cell of the fuel cell.

$$\dot{N}_{O_2,out,elect,sys} = \dot{N}_{O_2,in,fc}(n) \qquad \forall\, n \in N, n = 1 \tag{84}$$

The molar flow rate of O_2 consumed is given in Equation (85)

$$\dot{N}_{O_2,cons} = \frac{I(p)}{4F} \qquad \forall\, p \in P, p = fuel\ cell \tag{85}$$

Equation (86) states that the molar flow rate of O_2 leaving a cell is equal to the difference between the molar flow rate of O_2 entering the fuel cell, and the amount of O_2 consumed.

$$\dot{N}_{O_2,out,fc}(n) = \dot{N}_{O_2,in,fc}(n) - \dot{N}_{O_2,cons} \qquad \forall\ n \in N \tag{86}$$

Equation (87) states that the molar flow rate of O_2 in the cell *n* is equal to the molar flow rate of O_2 in the previous cell, i.e. *n*-1, of the fuel cell system.

$$\dot{N}_{O_2,in,fc}(n) = \dot{N}_{O_2,out,fc}(n-1) \qquad \forall\, n \in N, n > 1 \tag{87}$$

Equation (88) states that the molar flow rate of O_2 leaving the last cell in the fuel cell stack must be equal 0 to demonstrate that all O_2 produced in the electrolyser system is consumed.

$$\dot{N}_{O_2,out,fc}(n) = 0 \qquad \forall\, n \in N, n = |N| \tag{88}$$

3.5.3. Hydrogen Balance

The PEM is designed to allow H^+ ions to transfer from the anode to the cathode. Moreover, since the model being formulated is one-dimensional, no cross-permeation occurs. This means that the flow of H_2 into the anode compartment of the electrolyser is assumed to be negligible. H_2 in the fuel cell sub-system enters through the anode and is transferred through the membrane into the cathode, where H_2O is formed.

(11a)

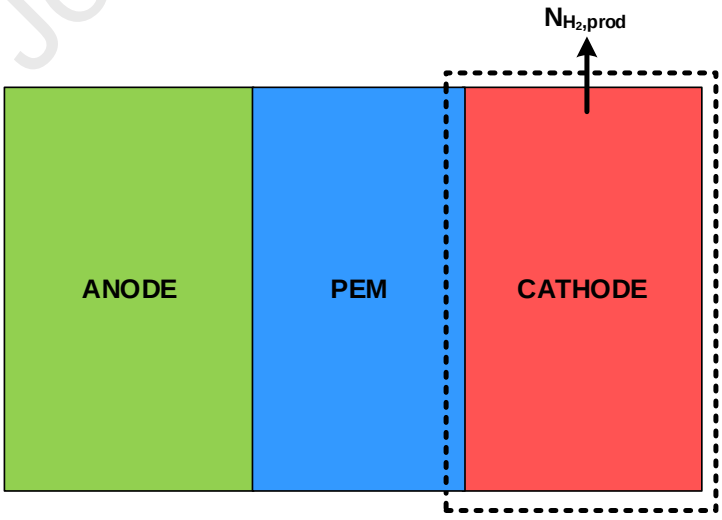

(11b)

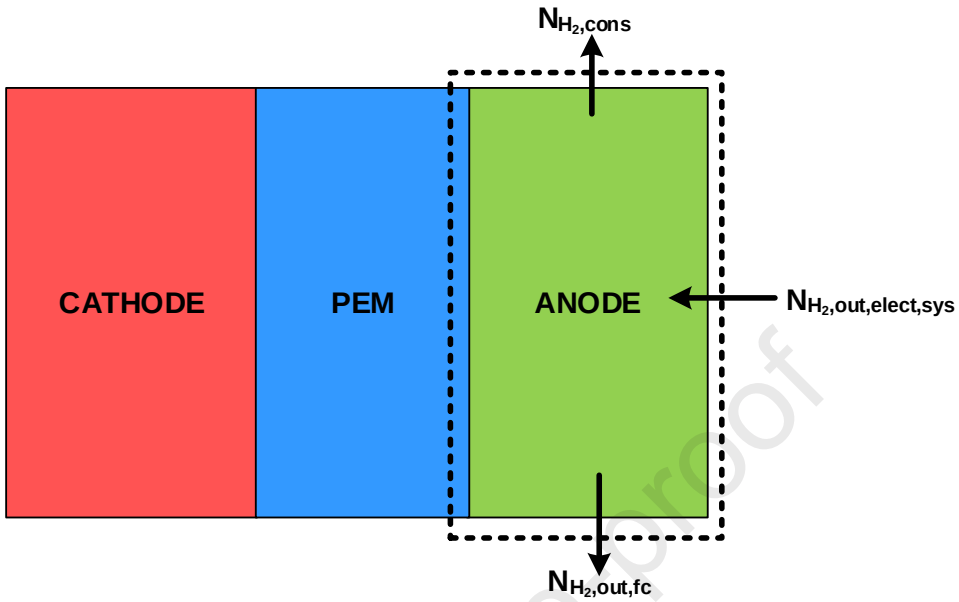

Figure 11: Hydrogen Balance across the Electrolyser (11a) and the Fuel Cell (11b)

The molar flow rate of H_2 produced in the electrolyser is given in Equation (89).

$$\dot{N}_{H_2,prod} = \frac{I(p)}{2F} \qquad \forall\, p \in P, p = electrolyser \tag{89}$$

Equation (90) states that the molar flow rate of H_2 leaving the cathode of the electrolyser is equivalent to the molar flow rate of H_2 produced.

$$\dot{N}_{H_2,out,cat,elect}(m) = \dot{N}_{H_2prod} \qquad \forall\ m \in M \tag{90}$$

The molar flow rate of H_2 leaving the electrolyser is given in Equation (91) and is equal to the molar flow rate of H_2 leaving the cathode of the electrolyser.

$$\dot{N}_{H_2,out,elect}\,(m) = \dot{N}_{H_2,out,cat,elect}(m) \qquad \forall\ m \in M \tag{91}$$

Equation (92) describes the total molar flow rate of H_2 leaving the system as the sum of all hydrogen molar flowrates leaving the electrolyser system.

$$\dot{N}_{H_2,out,elect,sys} = \sum \dot{N}_{H_2,out,elect}(m) \qquad \forall\, m \in M \tag{92}$$

The total molar flow rate of H_2 consumed is given in Equation (93).

$$\dot{N}_{H_2,cons} = \frac{I(p)}{2F} \qquad \forall\, p \in P, p = fuel\ cell \tag{93}$$

Equation (94) states that the total molar flow rate of H_2 leaving the electrolyser system is equal to the molar flow rate of H_2 entering the first cell of the fuel cell. It should be noted, that the molar flow rate of H_2 entering the cathode is assumed to be zero since H_2 is produced in the cathode.

$$\dot{N}_{H_2,out,elect,sys} = \dot{N}_{H_2,in,fc}(n) \qquad \forall\, n \in N, n = 1 \tag{94}$$

Equation (95) expresses the molar flow rate of H_2 as the difference between the molar mass of H_2 entering the fuel cell and being consumed.

$$\dot{N}_{H_2,out,fc}(n) = \dot{N}_{H_2,in,fc}(n) - \dot{N}_{H_2,cons} \qquad \forall\, n \in N \tag{95}$$

Equation (96) states that the molar flow rate of H_2 in the next cell is equal to the molar flowrate H_2 in the previous cell of the fuel cell system.

$$\dot{N}_{H_2,in,fc}(n) = \dot{N}_{H_2,out,fc}(n-1) \qquad \forall\, n \in N, n > 1 \tag{96}$$

Equation (97) states that the molar flow rate of H_2 leaving the last cell in the fuel cell stack must be equal 0, to demonstrate that all H_2 produced in the electrolyser system is consumed.

$$\dot{N}_{H_2,out,fc}(n) = 0 \qquad \forall\, n \in N, n = |N| \tag{97}$$

3.6. Overall System Performance

3.6.1. Total Power

The total power consumed and produced in the electrolyser and fuel cell systems are given in Equation (98) and (99). n_{cell} is the number of cells in the stacks.

$$Power_{cons} = \frac{V(p)*I(p)*n_{cell,elect}}{1{,}000} \qquad \forall\, p \in P, p = electrolyser \tag{98}$$

$$Power_{prod} = \frac{V(p)*I(p)*n_{cell,fc}}{1{,}000} \qquad \forall\, p \in P, p = fuel\ cell \tag{99}$$

3.6.2. Freshwater Recovery Rate

Equation (100) expresses the freshwater recovery rate in the HEFC system. It describes the percentage of seawater recovered as freshwater. FRR is the freshwater recovery rate.

$$FRR = \frac{N_{H_2O,prod}*n_{cell,fc}}{N_{H_2O,in,elect}} * 100 \tag{100}$$

3.6.3. Objective Function

The objective function in the HEFC system is to maximise the power conversion efficiency, which comprises of the power consumed, power produced and system efficiency. It is described in Equation (101).

$$\begin{aligned} obj &= \max\ (power\ conversion\ efficiency) \\ &= \max\ \left(\frac{Power_{prod}}{Power_{cons}} * \eta_{system}\right) \end{aligned} \tag{101}$$

3.7. Economic Evaluation

To conduct the economic evaluation, the fixed capital investment, replacement cost, maintenance cost and total annualised cost (TAC) equations are derived from the work done by Rahimi et al. (2014). Based on the TAC, revenue generated and total production cost, the annual cash flow, present values, net present value and payback period were calculated.

3.7.1. Fixed Capital Investment

The initial capital cost also known as fixed capital investment, is the amount of capital required to establish a chemical plant or business venture. It is comprised of the total direct capital cost and the total indirect capital cost. Equation (102) expresses the total direct capital cost required for the HEFC system, where $Cost_{stack}$ is the capital cost of the stack, $Cost_{BOP}$ is the capital cost of the balance of the plant, IF is the installation factor and CF_{land} is the land cost factor. Equations (103)-(104) give the cost of the stack and cost of the balance of the plant. CF_{stack} is the stack cost factor and CF_{BOP} is the balance of the plant cost factor. It should be noted that the capital cost of the electrolyser ($Cost_{cap,elect}$) and fuel cell ($Cost_{cap,fc}$) were extrapolated from the research conducted by Thomas (2018), whereby a graph had been constructed and a polynomial function obtained. The polynomial function obtained for the electrolyser and fuel cell is shown in Equations (105)-(106). Equation (107) gives the total capital cost ($Cost_{cap}$) for the HEFC system.

$$Cost_{TDC} = [(Cost_{stack} + Cost_{BOP}) * (1 + IF)] + (Cost_{cap} * CF_{land}) \quad (102)$$

$$Cost_{stack} = Cost_{cap} * CF_{stack} \quad (103)$$

$$Cost_{BOP} = Cost_{cap} * CF_{BOP} \quad (104)$$

$$Cost_{cap,elect} = \left(4.6 * Y_{purchase}{}^{2} - 18{,}658.2 * Y_{purchase} + 18{,}920{,}787\right) * Power_{cons} \quad (105)$$

$$Cost_{cap,fc} = \left(4.6 * Y_{purchase}{}^{2} - 18{,}658.2 * Y_{purchase} + 18{,}920{,}787\right) * Power_{prod} \quad (106)$$

$$Cost_{cap} = Cost_{cap,elect} + Cost_{cap,fc} \quad (107)$$

Equation (108) expresses the BOP cost factor. It is made up of the anode gas management system ($CF_{gms,an}$), cathode gas management system ($CF_{gms,cat}$), water delivery management system (CF_{dms,H_2O}), thermal management system (CF_{tms}), power electronics (CF_{pelect}), controls and sensors (CF_{cs}), mechanical BOP (CF_{MBOP}), other direct costs (CF_{other}) and assembly labour (CF_{AL}) cost factors.

$$CF_{BOP} = \begin{pmatrix} CF_{gms,an} + CF_{gms,cat} + CF_{dms,H_2O} + CF_{tms} \\ +CF_{pelect} + CF_{cs} + CF_{MBOP} + CF_{other} + CF_{AL} \end{pmatrix} \quad (108)$$

The indirect capital cost of the HEFC system is made up of the construction, engineering and design, project contingency, and the legal and contractor costs. Equation (109) describes the total indirect capital cost (C_{TIC}) of the HEFC system. $CF_{construction}$, CF_{ED}, CF_{PC} and CF_{LC} are the construction, engineering and design, project contingency, and legal and contractor fee cost factors.

$$C_{TIC} = [(CF_{construction} + CF_{PC} + CF_{LC}) * Cost_{TDC} + (CF_{ED} * Cost_{cap})] \quad (109)$$

Equation (110) expresses the fixed capital investment (FCI) required for the HEFC system.

$$FCI = C_{TDC} + C_{TIC} \quad (110)$$

3.7.2. Total Annualised Cost

The total annualised cost (TAC) describes the annual cost of owning, maintaining and operating the HEFC system over the lifetime of the plant. It comprises of the annualised capital cost($C_{Cap,annual}$), annualised replacement cost ($C_{Rep,annual}$) and the annualised maintenance cost ($C_{Main,annual}$). Equation (111) expresses the TAC of the HEFC system.

$$TAC\ (q) = C_{Cap,annual} + C_{rep,annual} + C_{main,annual} \qquad \forall\ q \in Q \qquad (111)$$

Equation (112) describes the total annualised capital cost of the system ($C_{Cap,annual}$). Y_{plant} is the plant lifetime and AI is the annual interest rate.

$$C_{Cap,annual} = \frac{(FCI*AI)(1+AI)^{Y_{plant}}}{(1+AI)^{Y_{plant}-1}} \qquad (112)$$

Similarly to the direct capital cost of the PEME and the PEMFC, the replacement cost is extrapolated from the research conducted by Thomas (2018). Equations (113)-(114) expresses the polynomial function obtained used to describe the replacement cost of the of the electrolyser and fuel cell. Where Y_{rep} is the year of replacement, $Cost_{rep,elect}$ is the replacement cost of the electrolyser and $Cost_{rep,fc}$ is the replacement cost for the fuel cell. Equation (115) gives the total replacement cost ($Cost_{rep}$) for the HEFC system. The annualised replacement cost is shown in Equation (116)

$$Cost_{rep,elect} = \left(4.6 * {Y_{rep}}^2 - 18{,}658.2 * Y_{rep} + 18{,}920{,}787\right) * Power_{cons} \qquad (113)$$

$$Cost_{rep,fc} = \left(4.6 * {Y_{rep}}^2 - 18{,}658.2 * Y_{rep} + 18{,}920{,}787\right) * Power_{prod} \qquad (114)$$

$$Cost_{rep} = Cost_{rep,elect} + Cost_{rep,fc} \qquad (115)$$

$$C_{rep\ ,annual} = \frac{Cost_{rep}*(1+IF)}{Y_{plant}} \qquad (116)$$

The annualised maintenance cost is considered to remain constant every year. In this paper, the annualised maintenance cost is taken as 2.5% of the initial capital cost.

3.7.3. Revenue and production costs

To determine the total revenue generated from the HEFC system, the income generated from the sale of freshwater and electricity are considered. Equation (117) states that the total income generated from the sale of water (Rev_{H_2O}) is equal to the mass flowrate of water ($M_{H_2O,out,fc,sys}$) multiplied by the cost of water ($Cost_{H_2O}$) and plant operating hours(Op_{hours}). Similarly, the sale of electricity (Rev_{elect}) is given in Equation (118).

$$Rev_{H_2O} = \left(\frac{M_{H_2O,out,fc,sys}}{\rho_{H_2O}}\right) * Cost_{H_2O} * Op_{hours} \quad (117)$$

$$Rev_{elect} = Power_{prod} * Cost_{elect} * Op_{hours} \quad (118)$$

Equation (119) gives the total revenue generated from the sale of water and electricity produced(Rev). In Equation (120) it is assumed that the revenue generated will annually increase at the same rate as the interest rate.

$$Rev(q) = Rev_{H_2O} + Rev_{elect} \qquad \forall\, q \in Q, q = 1 \quad (119)$$

$$Rev(q) = \left(Rev_{H_2O} + Rev_{elect}\right) + (1 + AI)^q \qquad \forall\, q \in Q, q > 1 \quad (120)$$

Equation (121) expresses the total production costs incurred in the HEFC system. CF_{PR}, CF_{ds}, CF_{RD} and CF_{ins} are the patent and royalty, selling and distribution, research and development, and insurance cost factors.

$$C_{TP}(q) = [(CF_{PR} + CF_{ds} + CF_{RD}) * Rev(q) + (FCI * CF_{ins})] \qquad \forall\, q \in Q \quad (121)$$

3.7.4. Cash Flow

The cash flow over the lifetime of the HEFC system is calculated in Equations (122) – (127). Equation (122) describes the depreciation(Dep) of the system and is calculated using the straight-line method. Equation (123) gives the profit before tax (PBT). Equation (124) indicates the amount of tax payable to the government(TAX). The profit after tax (PAT), profit after tax plus depreciation ($PATPD$) and annual cash flow ($CASH$) are given in Equations (125) - (127).

$$Dep\ (q) = \frac{FCI + Cost_{rep(1+IF)}}{Y_{plant}} \qquad \forall\ q \in Q \qquad (122)$$

$$PBT(q) = Rev(q) - C_{TP}(q) - Dep(q) \qquad \forall\ q \in Q \qquad (123)$$

$$TAX(q) = PBT(q) * Tax_{rate} \qquad \forall\ q \in Q \qquad (124)$$

$$PAT(q) = PBT(q) - TAX(q) \qquad \forall\ q \in Q \qquad (125)$$

$$PATPD(q) = PAT(q) + Dep(q) \qquad \forall\ q \in Q \qquad (126)$$

$$CASH(q) = PATPD(q) - TAC(q) \qquad \forall\ q \in Q \qquad (127)$$

3.7.5. Net Present Value

The net present value (NPV) gives the current value of operating the HEFC system over the lifetime of the plant. The discount factor (DF) is expressed in Equation (128) and is used to determine the present value of future cash flows. Equations (129) - (130) describe the present value (PV) and NPV of the proposed system.

$$DF(q) = \frac{1}{(1+AI)^{q-1}} \qquad \forall\ q \in Q \qquad (128)$$

$$PV(q) = CASH(q) * DF(q) \qquad \forall\ q \in Q \qquad (129)$$

$$NPV = \sum PV(q) \qquad \forall\, q \in Q \qquad (130)$$

3.7.6. Payback Period

Equation (131) gives the payback period of the plant, which states that the payback period is equal to the FCI multiplied by the plant life divided by the total revenue generated over the plant life.

$$PBP = \frac{FCI * Y_{plant}}{\sum Rev(q)} \qquad \forall\, q \in Q \qquad (131)$$

4. Illustrative Example

To illustrate the application of the HEFC system, the model is applied to the following illustrative example based on data extracted from literature, and are listed in Table 1 and Table 2. Table 3 and Table 4 lists the economic parameters and other cost factors that are considered

Table 1: Seawater Electrolyser and Hydrogen Fuel Cell Parameters

	Electrolyser		**Fuel Cell**	
	Value	**Reference**	**Value**	**Reference**
Inlet flowrate of seawater (mol/s)	0.01	-	-	-
Salinity (parts per thousand)	35	(Dresp et al., 2019)	-	-
Pressure (atm)	1		1	
Anode charge transfer coefficient	0.5	(Tijani et al., 2019)	0.5	(Tijani et al., 2019)
Cathode charge transfer coefficient	0.5	(Moradi Nafchi et al., 2019)	1	(Chowdhury et al., 2018)
Anode exchange current density (A/m^2)	13	(Bennett, 1980)	2 000	(Shimpalee and Van Zee, 2007)
Cathode exchange current density (A/m^2)	900	(Han et al., 2015)	200	(Shimpalee and Van Zee, 2007)
Membrane thickness (μm)	178	(Webster and Bode, 2019)	178	(Saebea et al., 2017)

Table 2: Economic Parameters (Colella et al., 2014)

Direct Costs	**Cost Factor**
Stack	38%
Hydrogen Gas Management System	6%
Oxygen Gas Management System	2%
Water Delivery Management System	5%
Thermal Management	5%
Power Electronics	26%
Controls and Sensors	6%
Mechanical Balance of the Plant	5%
Other Direct Costs	2%
Assembly Labor	5%
Land	4%
Installation Factor	10%

Indirect Costs	**Cost Factor**
Construction Costs	2%
Engineering and Design	8%
Project Contingency	15%
Legal and Contractor	15%

Table 3: Other Cost Factors and Rates

Other factors	**Value**	**Reference**
Working Capital	20%	(Turton, 2013)
Annual Interest Rate	6.75%	(Trading Economics, 2019)
Inflation Rate	4.5%	(SA Stats, 2020)
Maintenance Factor	2.5%	(Colella et al., 2014)
Purchase year	2019	-
Replacement year (10 years after purchase)	2029	(Colella et al., 2014)
Project life (years)	20	
Tax Rate	28%	(South African Revenue Services, 2020)

Table 4: Operating Condition Constraints

Variable	**Symbol**	**Electrolyser range**	**Fuel cell range**	**Reference**
Temperature (℃)	T	25-90	25-90	(Atyabi et al., 2019; Moradi Nafchi et al., 2019)
Current density (A/m^2)	i	>10,000 – 50.000-		(Abdel-Aal et al., 2010; Yan et al., 2019)
Voltage (V)	V	2.1-6	-	(Abdel-Aal et al., 2010)
Humidity degree	λ	14 - 25	14 - 25	(Han et al., 2015)
Electro-osmotic drag coefficient	n_d	>0.2	> 0.2	-
System efficiency (%)	η	67 - 82	67 - 82	(Valiollahi et al., 2019)
Power produced (kW)		-	1	-
Reaction area (cm^2)	A	50 - 400	50 - 400	-
Anode and cathode thickness (μm)	δ	50 – 6,250	50 – 6,250	-

To model the HEFC system, the following assumptions are made:

(i) The system operates in a continuous one-dimensional flow

(ii) The system operates under steady-state, isothermal and isobaric conditions at atmospheric pressure

(iii) PEME produces pure H_2 and O_2

(iv) All H_2O is present in the liquid phase

(v) Solar and wind energy are used to power the PEME

(vi) Cells are connected in series (current remains the same) and current is distributed uniformly

(vii) Gases behave as ideal gases

(viii) The pressure gradient between the anode and cathode is negligible

(ix) Uniform H_2O activity across the membrane

(x) No H_2O enters the PEMFC

(xi) No H_2 leaves the anode of the PEME and enters the cathode of the PEMFC

(xii) No O_2 leaves the cathode of the PEME and enters the anode of the PEMFC

(xiii) Chlorine leaves as a solution with excess seawater

(xiv) Auxiliary units such as heat exchangers, pumps and valves are not modelled. Therefore the power consumed by these units are not taken into account

(xv) System is operated for 8,000 hours/annum

5. Results and Discussion

The mathematical model of the HEFC system is implemented in GAMS 24.8.5 to maximise power conversion efficiency. BARON is used to solve the NLP optimisation problem. All results for the mathematical model were solved using a computer with the following specifications: Intel i7 processor on a Windows 7 Professional, 64-bit operating system with 8 GB of RAM.

Seawater is a solution of salts composed mainly of chloride, sodium, sulphate, magnesium, calcium, and potassium ions dissolved in H_2O. Since O_2 evolution is promoted over chlorine evolution, chlorine leaves the system as a solution with brine. This is achieved by operating the seawater electrolyser at current densities either below 1 mA/cm^2 which would require large electrode areas, or greater than 1,000 mA/cm^2 which would require more energy. In this study, current densities greater than 1,000 mA/cm^2 are used, as the cost required to power the electrolyser is not taken into account. This was based on solar and wind energy being readily available. The dissolved chlorine will take the form of hypochlorite, which is preferred compared to chlorine gas due to its non-toxic characteristics.

One of the major concerns facing seawater electrolysis is the deposition of magnesium hydroxide and calcium carbonate on the cathode. This generally occurs due to the rise in pH caused by the generation of H_2. Consequently, if precipitation deposit is not removed it will build up and prevent the efficient transfer of ions, which affects cell performance and efficiency (Badea et al., 2007). To account for this, precipitation removal costs are considered in the techno-economic evaluation. Furthermore, to overcome corrosion, platinum and nickel electrodes which are highly corrosion resistant are used to protect the electrode.

Since the HEFC system incorporates a seawater electrolyser and to the best of our knowledge, no mathematical models have been developed for a PEM seawater electrolyser, validating the entire model proved to be challenging. Therefore, each sub-system is validated separately.

5.1. Model Validation

To validate the seawater electrolyser, according to Zuttel et al. (2010), the minimum theoretical energy required at ambient conditions is 39.7 kWh/kg H_2. In this model, an energy requirement of 56.8 kWh/kg H_2 is achieved in the seawater electrolysis sub-system. This shows that the model is in fair agreement with the theoretical minimum energy requirement. Any deviations present may be attributed to the uncertainty in the type of electrolysis and water source used.

The present fuel cell model is validated with the simulation model developed by Adbin et al. (2016). As seen in Figure 12, the present model results are in fair agreement with the model developed by Adbin et al. (2016). However, the discrepancy at low current densities is large and may be due to the effect of the activity of H_2O, and the humidity degree of the anode-membrane and cathode-membrane interface, as well as the optimisation of the fuel cell in the HEFC system. In this model, the H_2O activity and the humidity degree expressions were adapted from Shimpalee and Van Zee (2007). At high current densities and low membrane humidity degrees, the ohmic overpotential is greater which means there is greater resistance for electrons to transfer through the membrane. As a result, the discrepancy between the two models is reduced. Additionally, the activation overpotential contributes to greater potential losses in the fuel cell. This may be due to the natural logarithmic function present in the activation overpotential, which is linearised in the proposed model. As a result, this reduces the output voltage of the fuel cell and leads to the nonlinear model presented by Abdin et al. (2016).

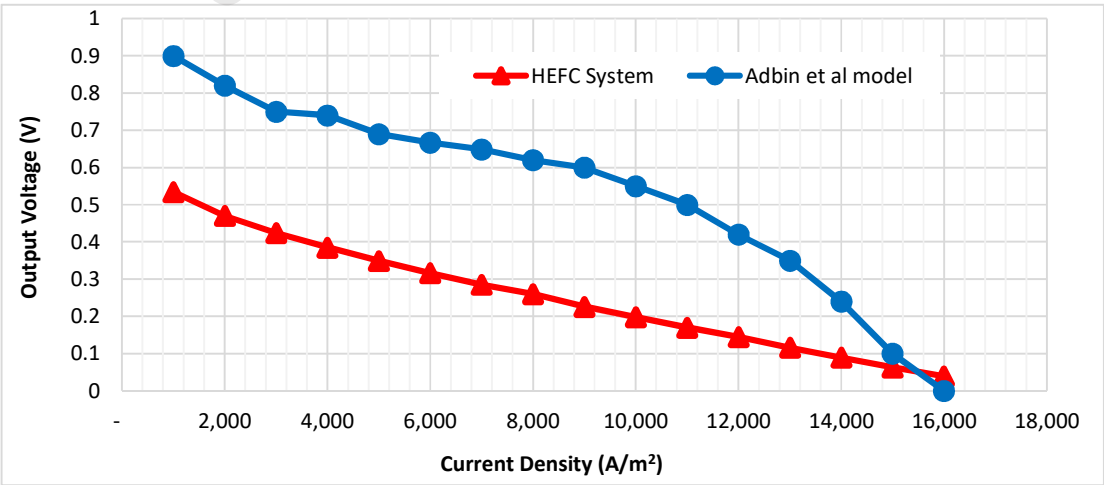

Figure 12: Fuel Cell Model Validation

5.2. Optimal Performance, Design Parameters and Operating Conditions

To determine the optimal number of cells in the fuel cell stack, the relationship between power conversion efficiency and the number of cells is evaluated. According to Figure 13, which is constructed from the current HEFC model, the optimal number of cells to maximise power conversion efficiency is 12 cells. The results reported hereafter will be based on a model formulated with 1 cell PEME cell and 12 PEMFC cells. Evidently, there is also an inverse relationship between power conversion efficiency and the water recovery rate.

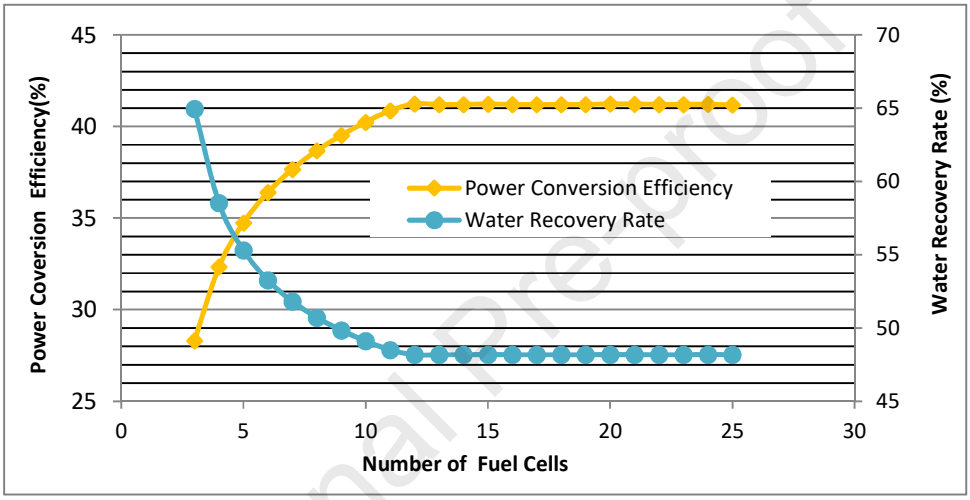

Figure 13: Relationship between Power Conversion Efficiency, Freshwater Recovery Rate and Number of Cells in the Fuel Cell Stack

Table 5: Optimal Performance Results for Each Cell

	Electrolyser	**Fuel cell**
Current density (A/m^2)	23,266	2,000
Open circuit voltage (V)	1.162	1.175
Activation overpotential (V)	0.654	0.067
Diffusion overpotential (V)	0	0
Ohmic overpotential (V)	0.323	0.031
Input voltage (V)	2.136	-
Output voltage (V)	-	1.076

From the results in Table 5, it can be seen that the diffusion overpotential does not affect the performance of the electrolyser and the fuel cell, due to the presence of a PEM electrolyte. The activation overpotential is found to be the main contributor to the voltage losses in the electrolyser and fuel cell. Additionally, due to the resistance in the flow of H^+ ions through the membrane, the ohmic overpotential is the second-largest source of potential loss.

Table 6: Optimal Design and Operating Conditions

	Electrolyser	**Fuel cell**
Temperature (℃)	80.1	66.7
Humidity degree	14.4	14.6
Electro-osmotic drag coefficient	1.64	0.20
Anode thickness (μm)	237	270
Cathode thickness (μm)	237	270
Reaction area (cm^2)	400	390

Table 6 shows that the optimal operating temperature when the electrolyser and fuel cell are operated under atmospheric pressure is 80.1 ℃ and 66.7 ℃. In literature, high temperatures (40-80℃) were found to improve the performance of both the PEME and PEMFC (Han et al., 2015). The optimal temperatures obtained from the model are in agreement with the observations made by Han et al. (2015), indicating that the electrolyser and fuel cell perform better at elevated temperatures. The humidity degree describes the amount of H_2O present in the membrane. Typically, a range of 14-25 is given, where 14 describes a fully saturated membrane and 25 is for a supersaturated membrane. From the results, the optimal humidification degrees are 14.4 and 14.6 in the electrolyser and fuel cell. This shows that adequate water management is required to prevent membrane dehydration and cathode flooding. If there is too little H_2O present in the membrane, membrane dehydration will occur and lead to lower performance. Additionally, cathode flooding will occur if there is excess H_2O present in the membrane. This will ultimately increase the resistance of the electrode. Consequently, the humidification degree is critical to the performance of the electrolyser and the fuel cell.

Table 7: Overall Results

Power conversion efficiency (%)	41.2
Freshwater recovery rate (%)	48.2
System Efficiency (%)	81.9
CPU Time (s)	0.03

Table 7 describes the overall results for the hybrid system. As seen, the power conversion efficiency of the system is 41.2 % and is produced from 100% green energy with 0% carbon emissions. Furthermore, 48.2 % of the seawater fed to the electrolyser is recovered as freshwater in the fuel cell. This H_2O recovered can be sent to the background process. By integrating the HEFC system with the background process, energy and H_2O can be produced on-site.

5.3. Economic Evaluation

Since in most instances, both good solar and wind resources are available, the power consumed in the electrolyser could be supplied by solar and wind energy. Recently, the cost-competitiveness of renewable enerergy shows remarkable transformation in the electricity generation sector. Typically, fossil fuel-derived power costs USD 0.04-0.14/kWh, compared to electricity generated from wind, which costs USD 0.04/kWh in the absence of financial support. Similary, in the solar and PV power generation industry, utility-scale electricity generation costs USD 0.069/kWh (Strielkowski, 2020). Conversely, in another report it has been reported that solar PV auction prices of USD 0.03/kWh are currently available (International Renewable Energy Agency, 2020). In this work the cost for renewable energy consumed was not taken into account, as the model was developed primarily for the optimal design and synthesis of the HEFC system. As such, the purpose of the model is to investigate operational feasibility of the proposed system in terms of power conversion efficiency. Therefore, no additional costs were assumed to be incurred to break down H_2O molecules, since the cost of electricity for the electrolyser was deemed negligible for the purposes of this study.

The basic cost factors used to breakdown the direct and indirect capital costs of various components in the HEFC system are obtained from Colella et al. (2014). Based on that work, the forecourts cost factors are used because the current HEFC system is modelled to have a 1 kW power production capacity. As a result, using the centralised production facility (CPF) cost factors would be inaccurate due to the large size variance between the HEFC system and the CPF.

The overall capital cost of the PEME is extrapolated from the research conducted by Thomas (2018). Based on that research, Figure 14 is constructed and a polynomial function is obtained. The PEME capital cost is expected to decrease over time, due to greater market uptake, higher production volumes, improved efficiencies, and cheaper catalysts and electrodes. It is important to note that Figure 14 is also used to determine the capital cost of PEMFCs, as PEMFC and PEME are constructed from similar components.

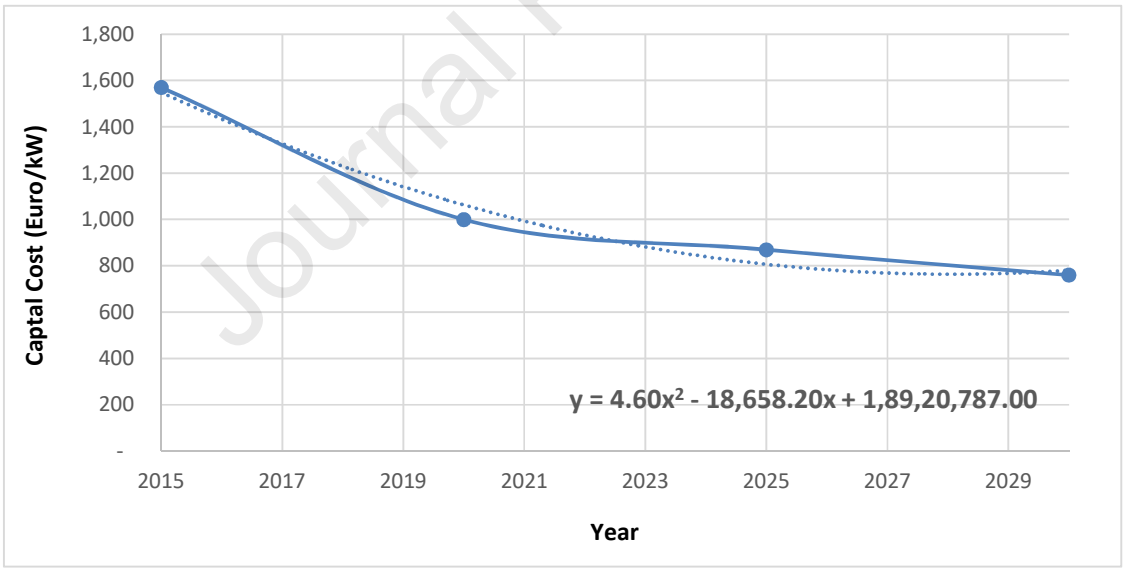

Figure 14: PEME and PEMFC Capital Cost from 2015-2030

Table 8: Techno-Economic Results

Total annualised cost (USD)	793
Internal rate of return (%)	16.3
Discount factor (%)	6.75
Payback period (years)	3.94
Net present value (USD)	1 498

The net present value (NPV) over a plant life of 20 years is positive indicating that the system generates enough income to compensate for all business risk. The payback period is 3.94 years. This is a good payback period as generally, a chemical plant design with a payback period of fewer than 5 years is accepted as being feasible (Sinnott, 2005). Subsequently, the system proves to provide an environmental benefit in addition to its financial prospects.

6. Conclusion

This work addresses the water crisis and energy trilemma that is affecting many countries globally. The proposed system models a hybrid electrolyser-fuel cell system to produce H_2 and freshwater from seawater. A one-dimensional, mathematical model operated under steady-state, continuous, isothermal and isobaric conditions have been developed for a HEFC system. The HEFC may be integrated with a background process to provide supplementary power. The hybrid system is modelled and optimised as an NLP problem in GAMS/BARON to maximise power conversion efficiency. Based on the results, 48.2 % of the seawater fed to the electrolyser is recovered as freshwater in the fuel cell. The hybrid system shows potential as being an efficient seawater purification system which releases 0% carbon emissions into the atmosphere. Additionally, it is environmentally friendly in its handling, production and use. As an energy conversion system, 41.2 % power conversion efficiency is achieved.

This indicates that the system shows promise of decentralising the production of electricity from fossil fuels, addressing the energy trilemma without straining freshwater bodies, and providing 100% clean supplementary power to background processes. In addition to its environmental benefits, the HEFC system is economically viable.

Some of the major limitations associated with the HEFC model include:

- Cross-permeation of H_2 and O_2 was not taken into account, as the system was modelled as a one-dimensional model. Two-dimensional and three-dimensional models can be developed to investigate the effect of cross-permeation on the performance of the system.
- The mathematical formulation of the seawater electrolyser was developed based on the parameters sourced from literature. It is not clear whether these parameters explicitly describe the seawater electrolysis operation under the conditions that were found to be optimal.
- This model does not take into account the operating costs of the renewable power consumed. This may be considered for future work whereby the objective function is comprised of economic constraints and variables.
- It should be noted that the power consumed by auxiliary units such as pumps, compressors and heat exchangers were not taken into account.
- The proposed system was conducted on PEME and PEMFCs. Therefore, investigations on the optimal performance of other types of electrolysers and fuel cells were not taken into account.

The overall perspective of this work is to illustrate the optimal design of a HEFC system to produce H_2 and freshwater from seawater, as well as the viability of the system. The results from the mathematical model provide insight into the efficiency and performance of the system, and can provide a better understanding of seawater electrolysis and the proposed hybrid system.

Acknowledgements

The financial support from the National Research Foundation (NRF) Research Chair in Sustainable Process Engineering (grant number: 47440) is gratefully acknowledged.

Nomenclature

Parameters

A_{H_2O}	Activity of water	-
α	Charge transfer coefficient	-
AI	Annual interest rate	-
C	Concentration	mol/m^3
CF	Cost factor	-
P_{cr}	Critical pressure	MPa
T_{cr}	Critical temperature	K
D	Diffusion coefficient	m^2/s
D_{eff}	Effective diffusion coefficient	m^2/s
j_o	Exchange current density	A/m^3
F	Faraday's constant	C/mol
IR	Inflation Rate	-
IF	Installation factor	-
δ_{mem}	Membrane thickness	μm
M_m	Molar mass	kg/mol
$M_{m,mem,dry}$	Molar mass of the dry membrane	kg/mol
n_{cell}	Number of cells	
z	Number of electrons transferred	
P	Pressure	MPa
P_{ref}	Reference pressure	MPa
T_{ref}	Reference temperature	K
R	Universal gas	J/$mol.K$
Tax_{rate}	Tax rate	
D_w	Water diffusion coefficient	m^2/s
K_{darcy}	Water permeability coefficient	m^2
Y_{plant}	Plant life	-
$Y_{purchase}$	Purchase year	-
Y_{rep}	Replacement year	-

Variables

$Cash$	Cash flow	USD
$Cost$	Cost	USD
C_{cap}	Capital cost	USD
I	Current	A
j	Current density	A/m^2
Dep	Depreciation	USD
D	Diffusion coefficient	m^2/s
DF	Discount Factor	-
n_d	Electrostatic drag coefficient	-
FCI	Fixed capital investment	USD
D_{eff}	Effective diffusion coefficient	m^2/s
IRR	Internal rate of return	-
C_{main}	Maintenance cost	USD
M	Mass flow rate	kg/hr
$\dot{N}$	Molar flow rate	mol/s
n	Molar flux	$mol/m^2.hr$
y	Molar fraction	-
Op_{hours}	Operating hours	hr
NPV	Net present value	USD
PAT	Profit after tax	USD
$PATPD$	Profit after tax plus depreciation	USD
PBT	Profit before tax	USD
PBP	Payback period	yr
$Power$	Power	kW
PV	Present value	USD
A	Reaction area	m^2
C_{rep}	Replacement cost	USD
Rev	Revenue	USD
P_{sat}	Saturation pressure	MPa
Rev	Revenue	USD
T	Temperature	K

TAC	Total annualised cost	USD
TDC	Total direct costs	USD
TIC	Total indirect costs	USD
TP	Total production	USD
V	Voltage or overpotential	V

Greek Symbols

α	Charge transfer coefficient	
ρ	Density	kg/m^3
$\rho_{mem,dry}$	Density of dry membrane	kg/m^3
η	Efficiency	
λ	Humidity degree	
σ_{mem}	Membrane conductivity	$ohm^{-1}m^{-1}$
β	Partial pressure	MPa
ε_p	Percolation	
ε	Porosity	
δ	Thickness	m
μ	Viscosity	$kg.s/m^3$

Sets

M	Number of cells in electrolyser stack =1
N	Number of cells in fuel cell stack = 1,2,3,…,25
P	Units = Electrolyser, Fuel cell
Q	Number of plant operating years = 1,2,3,...,20

Subscripts

act	Activation
AL	Assembly labour
an	Anode
$annual$	Annual
BOP	Balance of Plant
cat	Cathode
cap	Capital
ch	Channel
ch, o	Channel at reference conditions
$construction$	Construction
$cons$	Consumed
cs	Control and sensors
$diff$	Diffusion
DC	Direct cost
dms	Delivery management system
DS	Distribution and selling
ED	Engineering and design
$elect$	Electrolyser
eo	Electro-osmotic drag
fc	Fuel cell
gms	Gas management system
H_2	Hydrogen
IF	Installation factor
ins	Insurance
LC	Legal and contractor fees
$land$	Land
mem	Membrane
me	Membrane-electrode interface
me, o	Membrane-electrode interface at reference conditions
$MBOP$	Mechanical balance of plant
ohm	Ohmic

ocv	Open circuit voltage
$other$	Other
O_2	Oxygen
$other$	Other direct costs
PC	Project contingency
pe	Pressure effect
PR	Patents and royalties
$pelect$	Power electronics
$prod$	Produced
RD	Research and development
sw	Seawater
$stack$	Stack
sys	System
tms	Thermal management system
H_2O	Water
$H_2 - H_2O$	Hydrogen-water mixture
$O_2 - H_2O$	Oxygen-water mixture

References

Abdel-Aal, H.K., Zohdy, K.M., Kareem, M.A., 2010. Hydrogen Production Using Sea Water Electrolysis. Open Fuel Cells J. 3, 1–7.

Abdin, Z., Webb, C.J., Gray, E.M., 2015. Modelling and simulation of a proton exchange membrane (PEM) electrolyser cell. Int. J. Hydrogen Energy 40, 13243–13257. https://doi.org/10.1016/j.ijhydene.2015.07.129

Abdin, Z., Webb, C.J., Gray, E.M.A., 2016. PEM fuel cell model and simulation in Matlab–Simulink based on physical parameters. Energy 116, 1131–1144. https://doi.org/10.1016/j.energy.2016.10.033

Acar, C., Dincer, I., 2020. The potential role of hydrogen as a sustainable transportation fuel to combat global warming. Int. J. Hydrogen Energy. https://doi.org/10.1016/j.ijhydene.2018.10.149

AlZahrani, A.A., Dincer, I., 2017. Thermodynamic and electrochemical analyses of a solid oxide electrolyzer for hydrogen production. Int. J. Hydrogen Energy 42, 21404–21413. https://doi.org/10.1016/j.ijhydene.2017.03.186

Atyabi, S.A., Afshari, E., Wongwises, S., Yan, W.M., Hadjadj, A., Shadloo, M.S., 2019. Effects of assembly pressure on PEM fuel cell performance by taking into accounts electrical and thermal contact resistances. Energy. https://doi.org/10.1016/j.energy.2019.05.031

Badea, G.E., Caraban, A., Cret, P., Corbu, I., 2007. Hydrogen Generation By Electrolysis of Seawater. Fascicle Manag. Technol. Eng. 6.

Bennett, J.E., 1980. Electrodes for generation of hydrogen and oxygen from seawater. Int. J. Hydrogen Energy 5, 401–408. https://doi.org/10.1016/0360-3199(80)90021-X

Bernardi, D.M., Verbrugge, M.W., 1991. Mathematical model of a gas diffusion electrode bonded to a polymer electrolyte. AIChE J. 37, 1151–1163. https://doi.org/10.1002/aic.690370805

Carylsue, 2016. 4 Billion People Face Water Scarcity [WWW Document]. URL https://blog.education.nationalgeographic.org/2016/02/15/4-billion-people-face-water-scarcity/ (accessed 3.18.18).

Chandesris, M., Médeau, V., Guillet, N., Chelghoum, S., Thoby, D., Fouda-Onana, F., 2015. Membrane degradation in PEM water electrolyzer: Numerical modeling and experimental evidence of the influence of temperature and current density. Int. J. Hydrogen Energy 40, 1353–1366. https://doi.org/10.1016/j.ijhydene.2014.11.111

Chowdhury, M.Z., Genc, O., Toros, S., 2018. Numerical optimization of channel to land width ratio for PEM fuel cell. Int. J. Hydrogen Energy. https://doi.org/10.1016/j.ijhydene.2017.12.149

Colella, W.G., James, B.D., Moron, J.M., Saur, G., Ramsden, T., 2014. Techno-economic Analysis of PEM Electrolysis for Hydrogen Production.

Darras, C., Bastien, G., Muselli, M., Poggi, P., Champel, B., Serre-Combe, P., 2015. Techno-economic analysis of PV/H2 systems. Int. J. Hydrogen Energy 40, 9049–9060. https://doi.org/10.1016/j.ijhydene.2015.05.112

Dresp, S., Dionigi, F., Klingenhof, M., Strasser, P., 2019. Direct electrolytic splitting of seawater: Opportunities and challenges. ACS Energy Lett. https://doi.org/10.1021/acsenergylett.9b00220

El-Dessouky, H.T., Ettouney, H.M., 2002. Fundamentals of Salt Water Desalination. Elsevier. https://doi.org/10.1016/B978-0-444-50810-2.X5000-3

Espinosa-López, M., Darras, C., Poggi, P., Glises, R., Baucour, P., Rakotondrainibe, A., Besse, S., Serre-Combe, P., 2018. Modelling and experimental validation of a 46 kW PEM high pressure water electrolyzer. Renew. Energy 119, 160–173. https://doi.org/10.1016/j.renene.2017.11.081

Falcão, D.S., Pinto, A.M.F.R., 2020. A review on PEM electrolyzer modelling: Guidelines for beginners. J. Clean. Prod. https://doi.org/10.1016/j.jclepro.2020.121184

Gerbi, G., 2017. SA Ranked 30th Driest Country in the World," Eyewitness Newse [WWW Document]. URL http://ewn.co.za/2017/11/28/sa-ranked-30th-driest-country-in-the-world (accessed 5.30.18).

Han, B., Steen, S.M., Mo, J., Zhang, F.Y., 2015. Electrochemical performance modeling of a proton exchange membrane electrolyzer cell for hydrogen energy. Int. J. Hydrogen Energy 40, 7006–7016. https://doi.org/10.1016/j.ijhydene.2015.03.164

International Energy Agency, 2019. Electricity Information: 2019 [WWW Document]. Stat. iea. URL https://www.iea.org/reports/electricity-information-2019 (accessed 1.14.20).

International Renewable Energy Agency, 2020. Renewable Power Generation Costs in 2019, International Renewable Energy Agency. International Renewable Enery Agency, Abu Dhabi. https://doi.org/10.1007/SpringerReference_7300

Kimura, F., Anbumozhi, V., Nishimura, H., 2019. Transforming and Deepening the ASEAN Community. Jakarta.

Kuang, Y., Kenney, M.J., Meng, Y., Hung, W.H., Liu, Y., Huang, J.E., Prasanna, R., Li, P., Li, Y., Wang, L., Lin, M.C., McGehee, M.D., Sun, X., Dai, H., 2019. Solar-driven, highly sustained splitting of seawater into hydrogen and oxygen fuels. Proc. Natl. Acad. Sci. U. S. A. https://doi.org/10.1073/pnas.1900556116

Lee, D., Hwang, B., Lim, D., Chung, H.-B., You, S.-E., Ku, Y.-M., Park, K., 2019. Transport of Water through Polymer Membrane in Proton Exchange Membrane Fuel Cells. Korean Chem. Eng. Res. 57. https://doi.org/10.9713/KCER.2019.57.3.338

Lei, D., Nie, M., Cao, Y., Zuo, W., Tian, X., Zhao, Z., Li, Q., 2018. Properties of AuPdPt-WC/C nanocomposite catalyst in simulated seawater solution for hydrogen evolution. Mater. Res. Innov. 22, 183–186. https://doi.org/10.1080/14328917.2017.1287491

Li, Y., Lv, H., 2018. The combined effects of water transport on proton exchange membrane fuel cell performance. Chem. Eng. Trans. 65, 691–696. https://doi.org/10.3303/CET1865116

Lin, M., Surya, V., Adi, K., Chang, C., 2015. Flexible Photovoltaics / Fuel Cell / Wind Turbine (PVFCWT) Hybrid Power System Designs 45, 559–564. https://doi.org/10.3303/CET1545094

Liu, W.H., Ho, W.S., Lee, M.Y., Hashim, H., Lim, J.S., Klemeš, J.J., Mah, A.X.Y., 2019. Development and optimization of an integrated energy network with centralized and decentralized energy systems using mathematical modelling approach. Energy. https://doi.org/10.1016/j.energy.2019.06.158

Log, T., 2018. Consumer grade weather stations for wooden structure fire risk assessment. Sensors (Switzerland). https://doi.org/10.3390/s18103244

López Ortiz, A., Meléndez Zaragoza, M.J., Collins-Martínez, V., 2016. Hydrogen production research in Mexico: A review. Int. J. Hydrogen Energy 41, 23363–23379. https://doi.org/10.1016/j.ijhydene.2016.07.004

Maleki, A., 2018. Design and optimization of autonomous solar-wind-reverse osmosis desalination systems coupling battery and hydrogen energy storage by an improved bee algorithm. Desalination. https://doi.org/10.1016/j.desal.2017.05.034

Mammar, K., Saadaoui, F., Laribi, S., 2019. Design of a PEM fuel cell model for flooding and drying diagnosis using fuzzy logic clustering. Renew. Energy Focus. https://doi.org/10.1016/j.ref.2019.06.001

Marangio, F., Santarelli, M., Calì, M., 2009. Theoretical model and experimental analysis of a high pressure PEM water electrolyser for hydrogen production. Int. J. Hydrogen Energy 34, 1143–1158. https://doi.org/10.1016/j.ijhydene.2008.11.083

Mohammad, M., Kaukhab, M., 2011. Prospects of Sea Water Electrolysis for the Production of Hydrogen: An Exploratory Study on the Electrolysis of Magnesium Chloride Solution in the Presence of Sulfur. J. Chem. Soc. Pakistan 166–170.

Moradi Nafchi, F., Afshari, E., Baniasadi, E., Javani, N., 2019. A parametric study of polymer membrane electrolyser performance, energy and exergy analyses. Int. J. Hydrogen Energy. https://doi.org/10.1016/j.ijhydene.2018.11.081

Ni, M., Leung, M.K.H., Leung, D.Y.C., 2006. Electrochemistry Modeling of Proton Exchange Membrane (PEM) Water Electrolysis for Hydrogen Production. WHEC 16, 13–16.

Pierucci, S., Klemeš, J.J., Piazza, L., Bakalis, S., Saebea, D., Patcharavorachot, Y., Hacker, V., Assabumrungrat, S., Arpornwichanop, A., Authayanun, S., 2017. Analysis of Unbalanced Pressure PEM Electrolyzer for High Pressure Hydrogen Production. Chem. Eng. Trans. 57. https://doi.org/10.3303/CET1757270

Prieto-Prado, I., Del Río-Gamero, B., Gómez-Gotor, A., Pérez-Báez, S.O., 2018. Water and energy self-supply in isolated areas through renewable energies using hydrogen and water as a double storage system. Desalination 430, 1–14. https://doi.org/10.1016/j.desal.2017.12.022

Rahimi, S., Meratizaman, M., Monadizadeh, S., Amidpour, M., 2014. Techno-economic analysis of wind turbine-PEM (polymer electrolyte membrane) fuel cell hybrid system in standalone area. Energy 67, 381–396. https://doi.org/10.1016/j.energy.2014.01.072

Ratshomo, K., Nembahe, R., 2016. South African Coal Sector Report Directorate : Energy Data Collection , Management and Analysis. Dep. Energy 1–34.

Ravichanran, S., Balaji, R., Kannan, B.S., Elamathi, S., Sangeetha, D., Lakshmi, J., Vasudevan, S., Sozhan, G., 2011. Sulfonated polystyrene-block-(ethylene-ran-butylene)-block-polystyrene (SPSEBS) membrane for sea water electrolysis to generate hydrogen, in: ECS Transactions. https://doi.org/10.1149/1.3565511

Rinkinen, J., Shove, E., Torriti, J., 2019. Energy fables: Challenging ideas in the energy sector, 1st Editio. ed, Energy Fables: Challenging Ideas in the Energy Sector. Routledge, London. https://doi.org/10.4324/9780429397813

SA Stats, 2020. Inflation edges up to 4,6% [WWW Document]. URL http://www.statssa.gov.za/?p=13127 (accessed 3.23.20).

Saebea, D., Patcharavorachot, Y., Hacker, V., Assabumrungrat, S., Arpornwichanop, A., Authayanun, S., 2017. Analysis of unbalanced pressure PEM electrolyzer for high pressure hydrogen production. Chem. Eng. Trans. https://doi.org/10.3303/CET1757270

Shekhar, K., 2013. An investigation into the minimum dimensionality required for accurate simulation of proton exchange membrane fuel cells by the comparison between 1 and 3dimension models. University of Cape Town.

Shimpalee, S., Van Zee, J.W., 2007. Numerical studies on rib & channel dimension of flow-field on PEMFC performance. Int. J. Hydrogen Energy. https://doi.org/10.1016/j.ijhydene.2006.11.032

Sinnott, R.K., 2005. Coulson and Richardson's: Chemical Engineering Design, in: Coulson and Richardson's Chemical Engineering. Elsevier Butterworth-Heinemann.

South African Revenue Services, 2020. COMPANIES, TRUSTS AND SMALL BUSINESS CORPORATIONS (SBC) [WWW Document]. URL https://www.sars.gov.za/Tax-Rates/Income-Tax/Pages/Companies-Trusts-and-Small-Business-Corporations.aspx

Springer, T.E., Wilson, M.S., Gottesfeld, S., 1993. Modeling and Experimental Diagnostics in Polymer Electrolyte Fuel Cells. J. Electrochem. Soc. https://doi.org/10.1149/1.2221120

Springer, T.E., Zowodzinski, T.A., Gottesfeld, S., 1991. Polymer Electrolyte Fuel Cell Model. J. Electrochem. Soc. https://doi.org/10.1149/1.2085971

Srisiriwat, A., Pirom, W., 2017. Feasibility Study of Seawater Electrolysis for Photovoltaic/Fuel Cell Hybrid Power System for the Coastal Areas in Thailand, in: IOP Conference Series: Materials Science and Engineering. https://doi.org/10.1088/1757-899X/241/1/012041

Strielkowski, W., 2020. Renewable energy sources, power markets, and smart grids, in: Social Impacts of Smart Grids. Elsevier Inc., pp. 97–151. https://doi.org/10.1016/b978-0-12-817770-9.00004-3

Thomas, D., 2018. Cost Reduction Potential for Electrolyser Technology, EY P2G Platform. Berlin.

Tijani, A.S., Ghani, M.F.A., Rahim, A.H.A., Muritala, I.K., Binti Mazlan, F.A., 2019. Electrochemical characteristics of (PEM) electrolyzer under influence of charge transfer coefficient. Int. J. Hydrogen Energy. https://doi.org/10.1016/j.ijhydene.2019.08.188

Tobaru, S., Conteh, F., Senjyu, T., 2017. Novel 100% renewable energy power system considering real-time pricing, in: 2017 IEEE 3rd International Future Energy Electronics Conference and ECCE Asia, IFEEC - ECCE Asia 2017. IEEE, Taiwan. https://doi.org/10.1109/IFEEC.2017.7992186

Trading Economics, 2019. South Africa Interest Rate [WWW Document]. URL https://tradingeconomics.com/south-africa/interest-rate

Turton, R., 2013. Analysis, Synthesis, and Design of Chemical Processes Fourth Edition, Journal of Chemical Information and Modeling. https://doi.org/10.1017/CBO9781107415324.004

Valiollahi, R., Vagin, M., Gueskine, V., Singh, A., Grigoriev, S.A., Pushkarev, A.S., Pushkareva, I. V., Fahlman, M., Liu, X., Khan, Z., Berggren, M., Zozoulenko, I., Crispin, X., 2019. Electrochemical hydrogen production on a metal-free polymer. Sustain. Energy

Fuels. https://doi.org/10.1039/c9se00687g

Webster, J., Bode, C., 2019. Implementation of a Non-Discretized Multiphysics PEM Electrolyzer Model in Modelica, in: Proceedings of the 13th International Modelica Conference, Regensburg, Germany, March 4–6, 2019. https://doi.org/10.3384/ecp19157833

Yan, Z., Song, L., Tang, M., Feng, Z., 2019. Oxygen Evolution Efficiency and Chlorine Evolution Efficiency for Electrocatalytic Properties of MnO 2 -based Electrodes in Seawater. J. Wuhan Univ. Technol. Mater. Sci. Ed. https://doi.org/10.1007/s11595-019-2016-z

Yang, S., Wang, Z., Han, Z., Pan, X., 2019. Performance modelling of seawater electrolysis in an undivided cell: Effects of current density and seawater salinity. Chem. Eng. Res. Des. https://doi.org/10.1016/j.cherd.2019.01.009

Yang, Z., Du, Q., Jia, Z., Yang, C., Jiao, K., 2019. Effects of operating conditions on water and heat management by a transient multi-dimensional PEMFC system model. Energy 183, 462–476. https://doi.org/10.1016/j.energy.2019.06.148

Yu, L., Zhu, Q., Song, S., McElhenny, B., Wang, D., Wu, C., Qin, Z., Bao, J., Yu, Y., Chen, S., Ren, Z., 2019. Non-noble metal-nitride based electrocatalysts for high-performance alkaline seawater electrolysis. Nat. Commun. https://doi.org/10.1038/s41467-019-13092-7

Züttel, A., Remhof, A., Borgschulte, A., Friedrichs, O., 2010. Hydrogen: The future energy carrier. Philos. Trans. R. Soc. A Math. Phys. Eng. Sci. https://doi.org/10.1098/rsta.2010.0113

Declaration of interests

☒ The authors declare that they have no known competing financial interests or personal relationships that could have appeared to influence the work reported in this paper.

☐The authors declare the following financial interests/personal relationships which may be considered as potential competing interests: